REPORT DOCUMENTATION PAGE

AFRL-SR-AR-TR-02-

0443

1. REPORT DATE (DD-MM-YYYY)	2. REPORT TYPE	3. DATES COVERED (From - To)
15 August 2002	Final Report	11/01/1999 - 10/31/2002

4. TITLE AND SUBTITLE
Radiation Effects on Space Based Optoelectronic Materials and Devices

5a. CONTRACT NUMBER

5b. GRANT NUMBER
F49620-00-0026 00-10026

5c. PROGRAM ELEMENT NUMBER

6. AUTHOR(S)
Omar Manasreh

5d. PROJECT NUMBER

5e. TASK NUMBER

5f. WORK UNIT NUMBER

7. PERFORMING ORGANIZATION NAME(S) AND ADDRESS(ES)

Department of Electrical and Computer Eng.
University of New Mexico
Albuquerque, NM 87131

8. PERFORMING ORGANIZATION REPORT NUMBER

9. SPONSORING / MONITORING AGENCY NAME(S) AND ADDRESS(ES)
Air Force Office of Scientific Research
801 N. Randolph St.
Arlington, VA 22203-1977

10. SPONSOR/MONITOR'S ACRONYM(S)
AFOSR/NE

11. SPONSOR/MONITOR'S REPORT NUMBER(S)

12. DISTRIBUTION / AVAILABILITY STATEMENT

Unlimited

13. SUPPLEMENTARY NOTE

14. ABSTRACT

We have investigated the irradiation effects on interband and intersubband transitions in III-V semiconductors quantum wells and superlattices. We also investigated irradiation induced defects in III-nitride thin films including C-H complexes in AlGaN. In particular, we investigated the Gamma-ray, electron, neutron, He^{+}-ion, and proton irradiation effects on the intersubband transitions in multiple quantum wells. Thermal annealing recovery of the intersubband transition (or thermal recycling) in heavily irradiated samples has been investigated. The final report contains detail discussions of the results obtained during the last three years. At the end of the report, we listed our professional activities including technical papers, books, symposia, invited talks, and students supported by the grant.

15. SUBJECT TERMS
Radiation effects, Long Wavelength Infrared Detectors, Optoelectronic Materials and Devices, III-V Quantum Wells and Superlattices.

16. SECURITY CLASSIFICATION OF:			17. LIMITATION OF ABSTRACT	18. NUMBER OF PAGES	19a. NAME OF RESPONSIBLE PERSON
			None		Omar Manasreh
a. REPORT	b. ABSTRACT	c. THIS PAGE			19b. TELEPHONE NUMBER (include area code)
Unclassified	Unclassified	Unclassified			(505) 277-3688

Standard Form 298 (Rev. 8-98)
Prescribed by ANSI Std. Z39.18

20030115 100

FINAL REPORT

RADIATION EFFECTS ON SPACE-BASED OPTOELECTRONIC MATERIALS AND DEVICES.

AFOSR Grant number F49620-00-0026

Prepared by

Dr. Omar Manasreh
Depart of Electrical & Computer Engineering, EECE Building, Room 320 C
University of New Mexico, Albuquerque, NM 87131-1356
Phones: Office: (505)277-3688, Mobile: (505) 463-3688,
FAX: (505)277-1439, E-Mails: manasreh@eece.unm.edu

Submitted to

LtCol Todd D. Steiner, PhD
Program Manager, Optoelectronic Materials Physics and Electronics Directorate
Air Force Office of Scientific Research
801 N Randolph St, Arlington VA 22203
Phone: 703 696 7314, Fax 703 696 8481
email: todd.steiner@afosr.af.mil

TABLE OF CONTENTS

1. INTRODUCTION:

Irradiation-induced defects in bulk III-V semiconductors have been the subject of many research interests in the last three decades or so. However, the irradiation effect on interfaces in superlattices and heterojunctions and on various transitions, such as intersubband and interband transitions, in multiple quantum wells have received little attention thus far. Gamma-ray, electron, neutron, and proton irradiation effects on the intersubband transitions in InGaAs/AlGaAs multiple quantum wells have been recently reported. A recent report on the proton irradiation effect on GaAs quantum well lasers indicates that there is a wavelength shift in the lasing spectra.

The interest in irradiation effects on multiple quantum wells and superlattices spurs from the fact that many devices based on III-V semiconductor quantum wells and superlattices are components in systems used for space applications. For example, focal plane arrays fabricated from GaAs related multiple quantum wells for long wavelength application is a sensor used in space for various applications. The prolonged operation of such devices in space environment may results in degradation due to electron, proton, neutron and gamma-ray radiation. Thus, it is desired to study multiple quantum well structures that form the basis of long wavelength infrared detectors, under the influence of various radiation effects.

Proton irradiation effect on the intersubband transitions in III-V semiconductor quantum wells is investigated thoroughly during the last three years. The desire to study this effect is based on two-folds. First, intersubband transitions form the basis of a new generation of long and very long wavelength infrared detectors. Second, space application is one of the most recent uses of this class of detectors, hence the survivability of these detectors in space and radiation environment becomes very important. Charge ionization and atomic displacement are the most important effects in irradiated semiconductor materials and devices. Charge ionization plays a major role in the device performance since irradiation induced charge-accumulation has a detriment effect on electronic and optoelectronic devices. Generally speaking, the charge ionization effect is sensitive to the temperature (T_i) at which the irradiation is performed. On the other hand, irradiation induced atomic displacement affect both devices and materials. It is more profound at high doses and less sensitive to T_i.

2. Photoluminescence Measurements of Interband Transition in Fast Neutron Irradiated $In_{0.07}Ga_{0.93}As/Al_{0.4}Ga_{0.6}As$ Multiple Quantum Wells:

In this section, we present photoluminescence (PL) measurements of interband transitions in InGaAs/AlGaAs multiple quantum wells before and after fast neutron irradiation. We will provide possible explanations to the degradation of interband transition as the irradiation dose is increased. The degradation of the interband transition was judged from the dramatic reduction of the normalized integrated area as well as the shift in the peak position energy of the PL spectra.

The multiple quantum well (MQW) structure used in the present study was grown by the molecular-beam epitaxy technique on a semi-insulating GaAs substrate. The wafer consists of 50 periods of 75 Å thick $In_{0.07}Ga_{0.93}As$ well and 100 Å thick

$Al_{0.4}Ga_{0.6}As$ barrier. The well regions were Si-doped {[Si] = $2x10^{18}$ cm^{-3}}. The uniformity of the wafer was determined from the peak position of the intersubband transition measurements to be within less than 0.5 meV in samples cut from the center and edge of the wafer. Several samples were cut and irradiated with different doses of fast neutrons beam. An unirradiated sample cut from the same wafer was used in other studies. The photoluminescence measurements were performed after cooling the sample to a temperature of 25 K using a conventional set-up.

It was determined that the MQW structure used in the present study possesses three confined energy levels (E_1, E_2, and E_3) in the quantum wells. Based on the doping level in the quantum well regions, it was also determined that the Fermi energy level is located above E_1 and well below E_2. Thus, one intersubband transition between the ground and first excited states (E_{12}, i.e E_1 to E_2) should be observed in the optical absorption spectrum of the reference sample. Indeed, this transition was observed and reported in the next section. On the other hand, the PL spectrum is originated from the electrons as they decay from E_1 to the heavy hole ground state (HH_1) after they were excited by the laser. The result is shown in Fig. 1 [see spectrum (a)]. This spectrum appears to be composed of two peaks; one is related to E_1 to HH_1 transition (the peak at around 1.5 eV) and the other transition (the peak around 1.488 eV) is possibly related to the conventional band edge transition in the GaAs substrate. Spectra (b), (c), (d), and (e) in Fig. 1 were obtained for samples irradiated with fast neutrons at four different doses of $4.20x10^{14}$ cm^{-2}, $1.20x10^{15}$ cm^{-2}, $3.60x10^{15}$ cm^{-2}, and $1.08x10^{16}$ cm^{-2}, respectively. It is clear from this figure that the peak at 1.488 eV, which is presumably related to the band edge of the GaAs substrate, is almost disappeared in the spectra of the irradiated samples. Additionally, the intensity of the PL peak related to the E_1 to HH_1 transition is dramatically reduced. The normalized total integrated area (I/I_0) of the PL spectra in Fig. 1 is plotted as a function of the irradiation dose and shown in Fig. 2, where I is the total integrated area obtained for the PL spectra of the irradiated samples and I_0 is the total integrated area of the PL spectrum of the unirradiated sample.

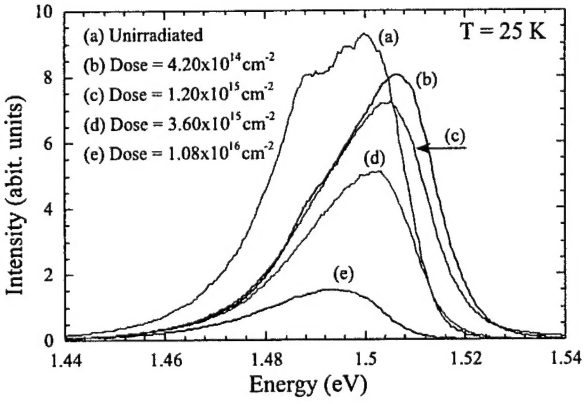

Fig. 1. Photoluminescence spectra obtained at T = 25 K and plotted as a function of fast neutron irradiation dose. Spectrum (a) was obtained for the reference sample (unirradiated). The rest of the spectra were obtained for samples irradiated with different doses as indicated.

The normalized integrated area seams to be decreased exponentially as the irradiation dose is increased. The reduction of I/I_0 reflects the decrease of the number of electrons that undergo the interband transition. It is also an indication that the density of state in the conduction band quantum well is reduced due to the irradiation-induced

damages at the interfaces. The reduction of the density of states limits the number of electrons excited by the laser to jump from the valence band to the conduction band leading to a significant loss of the PL intensity.

It is noted that the peak position energy of the PL spectra is affected as the irradiation dose is increased as shown in Fig. 3. At first, the peak position energy is increased from 1.499 eV for the unirradiated sample to 1.506 eV for the sample irradiated with a dose of 4.2×10^{14} cm^{-2}. Then the peak position energy starts to decrease as the irradiation dose is increased. This behavior could be explained as follows. It is well known that many body effects, in particular exchange interaction and depolarization effect, play a major role in the shifting of the quantized energy levels in the multiple quantum wells. It was determined that the ground state in the quantum well conduction band is lowered as the electron density is increased. It was also observed that the peak position energy of the PL spectrum of the E_1 to HH_1 transition is decreased approximately linearly as the doping level is increased in p-type Be doped GaAs/AlGaAs

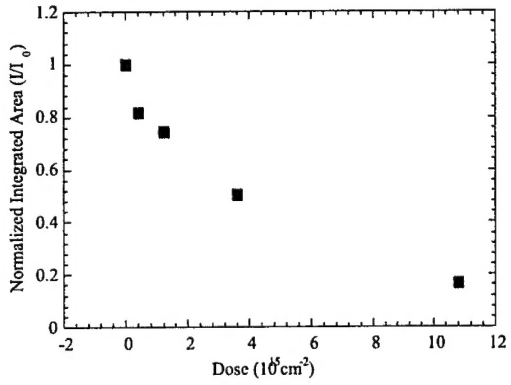

*Fig. 2. Normalized integrated area (I/I_0) of the PL spectra plotted as a function of the fast neutron irradiation dose. I_0 is the integrated area of spectrum (a) and I is the integrated area for spectra (b) - (e) in Fig. 1.*as

multiple quantum wells. In addition, fast neutron irradiation tends to bring the Fermi energy level toward the center of the band gap due to the fact the many irradiation-induced point defects such as antisites and vacancies act as electron traps. This leads to the reduction of the two-dimensional electron gas density in the conduction band quantum wells. Hence, the ground sate (E_1) in the conduction band is shifted toward a higher energy. Accordingly, the separation between E_1 and HH_1 is increased leading to an increase in the peak position energy of the PL spectra as illustrated in Figs. 1 and 3.

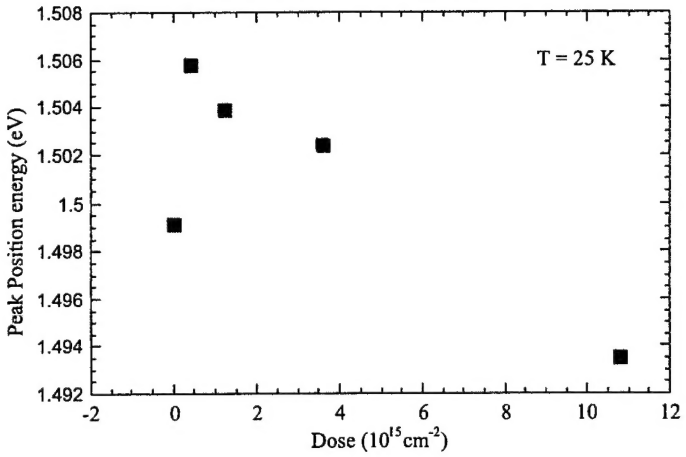

Fig. 3. The peak position energy of the spectra reported in Fig. 1 plotted as a function of the fast neutron irradiation dose.

After the initial increase of the peak position energy of the PL spectrum of the irradiated sample (dose = $4.20\text{x}10^{14}$ cm^{-2}) as shown in Fig. 3, the peak position energy starts to decrease as the irradiation dose in increased. It is even noted that the peak position energy of sample irradiated with a dose of $1.08\text{x}10^{16}$ cm^{-2} is lower than that of the unirradiated sample (reference sample). It is more difficult to explain this behavior. However, one possible explanation is that the high doses of fast neutron irradiation produces extensive damage at the InGaAs well and AlGaAs barrier interfaces such that the ground states (E_1 and HH_1) in both the conduction and valence band quantum wells are brought closer toward the bulk conduction and valence bands maxima of the quantum well material. This leads to a significant red-shift of the PL peak position energy.

Photoluminescence measurements for the interband transition in fast neutron irradiated $In_{0.07}Ga_{0.93}As/Al_{0.4}Ga_{0.6}As$ multiple quantum well samples are reported in this section. The PL spectra exhibit a significant degradation in heavily irradiated samples. The peak position energy of the PL spectra was observed to increase and then decrease as the irradiation dose is increased. The reduction of the normalized integrated area and the behavior of the peak position energy of the PL spectra as a function of the irradiation dose were interpreted as being due to the introduction of the irradiation-induced defects in the quantum well and barrier regions as well as due to the damages introduced at the well/barrier interfaces.

3. Electron Irradiation Effects on the Intersubband Transitions in InGaAs/AlGaAs Multiple Quantum Wells:

In this section, we report on the electron irradiation effect on the intersubband transitions in n-type $In_{0.07}Ga_{0.93}As/Al_{0.4}Ga_{0.6}As$ multiple quantum wells. It will be shown that the intensity of the intersubband transitions is dramatically decreased in heavily irradiated samples, which can be explained in terms of trapping of the two-dimensional electrons by the irradiation induced defects. A negative persistent effect was also observed in the heavily irradiated samples. It is noted that the recovery of the electrons

from this effect occurs at two temperature stages with thresholds at ~140 K and ~250 K, which indicates that the electrons were released from two different traps as the temperature is increased.

The multiple quantum well (MQW) structure used in the present study was grown by the molecular-beam epitaxy technique on a semi-insulating GaAs substrate. The wafer consists of 50 periods of 117 Å thick $In_{0.07}Ga_{0.93}As$ well and 100 Å thick $Al_{0.4}Ga_{0.6}As$ barrier. The well regions were Si-doped {[Si] = $2x10^{18}$ cm^{-3}}. Several samples were cut and irradiated with different doses of either 2 MeV or 5 MeV electrons beams. An unirradiated sample cut from the same wafer was used in other studies. The infrared absorption spectra were recorded at the Brewster's angel of GaAs (73°) from the normal using a BOMEM Fourier-transform interferometer in conjunction with a continuous flow cryostat. The temperature was controlled within ±1.0 K.

It was determined from a previous measurements that the MQW structure used in the present study possesses three confined energy levels (E_1, E_2, and E_3) in the quantum wells. Based on the doping level in the quantum well regions, it was also determined that the Fermi energy level is slightly above the first excited sate (E_2). Thus, two intersubband transitions between the ground and first excited states ($E_{12} \equiv E_1$ to E_2) and between the first and second excited states ($E_{23} \equiv E_2$ to E_3) should be observed in the optical absorption spectrum of the reference sample (unirradiated). Indeed, we have observed these two transitions in spectrum (a) as shown in Fig. 4. This spectrum was obtained at room temperature and it exhibits two peaks at ~ 780 cm^{-1} and ~ 980 cm^{-1}, which are assigned to E_{12} and E_{23} transitions, respectively. Spectrum (b) in Fig. 4 was obtained for the reference sample at T = 77 K. The peak position energies of both transitions have been shifted toward higher energies as the temperature is decreased. This effect has been the subject of a previous study. It is also observed that the intensity of E_{12} transition is increased while the intensity of the E_{23} transition is decreased as the temperature is decreased. This behavior can be easily explained in terms of phase blocking and the dropping of the Fermi energy levels as the temperature is reduced from room temperature to 77 K.

Spectrum (c) in Fig. 4 was obtained for a sample cut from the same wafer and irradiated with 2 MeV electrons beam. The irradiation dose was 5 $x10^{17}$ cm^{-2}. This spectrum exhibits only one transition related to E_{12}. The intensity of this transition is much smaller that that of the reference sample. The E_{23} transition was not observed in the irradiated sample. Similar behaviors were observed in other samples irradiated with the same electrons beam but with irradiation doses ranging from (1 - 4)$x10^{17}$ cm^{-2}. However, samples irradiated with 5 MeV electrons beam and doses ranging between $2.0x10^{10}$ cm^{-2} and $1.0x10^{12}$ cm^{-2} show only a slight difference between their spectra and the reference sample's spectrum. Spectrum (d) is the same as spectrum (c), but it was obtained at 77 K. The intensity of the E_{12} transition in spectrum (d) is reduced dramatically, but the transition remains observable. Similar results were obtained in samples irradiated with doses of (1 - 4)$x10^{17}$ cm^{-2}.

It is also observed in Fig. 4 that the peak position energy of the E_{12} transition in the irradiated sample experiences a much smaller shift with temperature than the unirradiated sample. This behavior could be explained as follows. The total integrated area of the intersubband transition is reduced in the irradiated sample, which is an indication that the total number of electrons that undergo this transition is reduced by the trapping mechanism due to the presence of the irradiation-induced defects. It was also observed previously that the temperature blue-shift in the intersubband transition is reduced as the electron density in the quantum well is decreased. Thus, the smaller shift with temperature in the irradiated sample as compared to that of the unirradiated sample can be easily explained in terms of the reduction of the electron density, which in turns reduce many-body effects on the peak position of the intersubband transition.

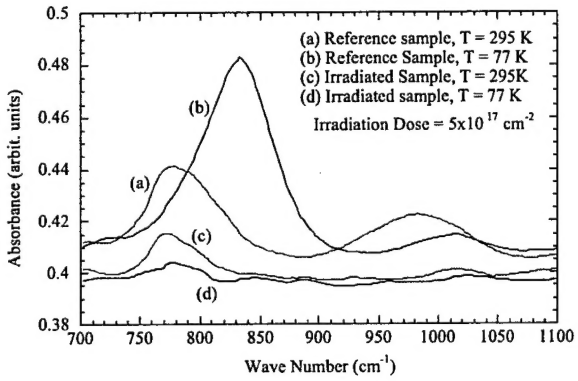

Fig. 4. Optical absorption spectra of intersubband transitions in InGaAs/AlGaAs multiple quantum wells measured at 295 K and 77 K. Spectra (a) and (b) were obtained for a reference sample (unirradiated) and spectra (c) and (d) were obtained for a sample irradiated with 2 MeV electrons beam and a dose of $5x10^{17}$ cm^{-2}.

The total integrated area of the E_{12} transition in the irradiated sample, which is shown in spectra (c) and (d) in Fig. 4, is studied as a function of temperature. The results are presented in Fig. 5. The total integrated area remains approximately constant between 77 K and 140 K. A sudden increase in the total integrated area is observed around 150 K. A change of the slope of the integrated area as a function of temperature is also observed at around 250 K.

It is clear from the present results that the electron irradiation with high doses has a drastic effects on the intersubband transitions in InGaAs/AlGaAs multiple quantum wells. Electron irradiation in III-V semiconductors is well known to produce point and complex defects such as antisites, vacancies, interstitials, and various combinations of point defects. In addition, it is anticipated that electron irradiation induced defects may have adverse effects on the interfaces in heterostructures which leads to alternations in the confined energy levels and the two-dimensional electron (hole) gas. Consequently, the interband and intersubband transitions in quantum wells and heterostructures are affected by electron irradiations.

The difference between the intersubband transitions spectra, shown in Fig. 4, in samples before and after electron irradiation can be explained as follows. Antisites, interstitials, and vacancies are the primary point defects introduced by electron irradiation. These point defects may form complex defects such as antisite-vacancy, Frenkel pair defects, etc. However, the five primary electron traps in electron irradiated

GaAs are E1, E2, E3, E4, and E5. These defects, in particular, E1, E2, and E3 produce energy levels close to the conduction band, which act as electron traps. Thus, by irradiating the InGaAs/AlGaAs MQWs with 2 MeV electrons and doses higher than $1x10^{17}cm^{-2}$, one can introduce various defects and electron traps, which can capture the electrons from the InGaAs quantum wells. The reduction of the two-dimensional electrons gas in the quantum wells can be probed by measuring the optical absorption of the intersubband transitions. By inspecting the spectra in Fig. 4, one can see the following: First, the total integrated area of E_{12} transition measured at 77 K is greatly reduced as illustrated in this figure by comparing spectra (b) and (d), which are obtained for the reference and irradiated samples, receptively. Second, the E_{23} transition is not observable in the spectra of the irradiated sample, which indicates that the Fermi energy level is dropped well below the first excited state (E_2). However, it should be pointed out that mixing between the quantum well and the barrier may occur in the irradiated sample , which may cause the suppression of the E_{23} transition. This possibility requires further studies. Third, the peak position energy of the E_{12} transition in the reference sample [spectrum (b)] is shifted from ~ 830 cm^{-1} to ~ 770 cm^{-1} in the irradiated sample [spectrum (d)]. This red-shift indicates that the many-body effects, which depend strongly on the two-dimensional electron gas density, is reduced among electrons in the quantum wells. The above three points strongly suggest that the electrons in the quantum wells are removed from the well through trapping and capturing by irradiation induced defects.

The total integrated area (I) of the E_{12} transition in the irradiated sample [see spectrum (c) in Fig. 4] was tracked as a function temperature as shown in Fig. 5. It is

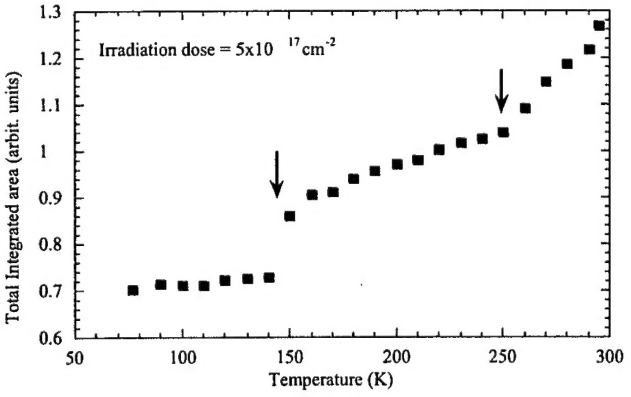

Fig. 5. The total inteegrated area of the intersubband transition between the ground and first excited states in the electron irradiated InGaAs/AlGaAs multiple quantum wells measured as a function of temperature. The vertical arrows indicate the threshold temperatures at which the electrons are released from the irradiation induced traps to the quantum wells.

well known that I is directly proportional to the two-dimensional electron gas density (σ) according to the following equation[13].

$$I \approx \frac{N\sigma L e^2 h}{4\varepsilon_o m^* c} \frac{f}{n^2(n^2+1)^{1/2}}, \quad (1)$$

where N is the number of the wells, L is the well width, m* is the electron effective mass, n is the refractive index of the well materials, and f is the oscillator strength. Thus, the measurement of the total integrated area provides a direct monitoring of the total number of electrons that undergo intersubband transitions.

The partial recovery of I around 150 K in Fig. 5 is similar to the recovery of the two-dimensional electrons gas in the negative persistent photoeffect observed in heavily doped n-type GaAs/AlGaAs multiple quantum wells, which is opposite to the positive persistent photoeffect usually associated with the DX center. However, the effect observed around 150 K in Fig. 5 is not a photoeffect. We may define it as a negative persistent temperature effect, since a secondary light illumination was not used in the present study and the intensity of the globar light source in the interferometer was too weak to cause any persistent photoeffects. The fact that we observe a partial recovery around 150 K in Fig. 2 is an indication that the electrons may have been released from a Si-related complex defect.

The change of the slope of the data around 250K as shown in Fig. 5, suggests that another shallow defects is involved in capturing the electrons as the temperature is decreased and then releasing them as the temperature is increased. It is difficult to identify the atomic structure of this trap, but it may be related to an arsenic vacancy. This speculation is based on the theoretical calculations of the electronic energy levels of the arsenic vacancy and the arsenic vacancy-gallium antisite pair defects.

We presented in this section new results on the behavior of the intersubband transitions in InGaAs/AlGaAs multiple quantum wells under the influence of 2 MeV electrons irradiation. It is observed that the total integrated area of the intersubband transitions are dramatically decreased after irradiating the samples with doses higher than $1x10^{17}$ cm^{-2}. This reduction was interpreted as being due to the trapping of the two-dimensional electrons gas by the irradiation induced-defects. The total integrated area of the intersubband transition between the ground and first excited state was studied as a function of temperature. The results revealed that two irradiation induced traps are involved in capturing the electrons as the temperature is lowered to 77 K. The electrons are then released from the traps as the temperature is increased to 300 K in two stages with thresholds around 140 K and 250 K.

4. Proton Irradiation Effects on the Intersubband Transition in GaAs/AlGaAs Multiple Quantum Wells with Bulk or Superlattice Barriers:

In this section, we report on the proton irradiation effect on optical absorption spectra of the intersubband transitions in n-type GaAs/AlGaAs MQWs. It will be shown that the intensity of the intersubband transitions is dramatically decreased as a function of irradiation doses, which can be explained in terms of trapping of the two-dimensional electrons in the quantum wells by the irradiation induced defects. In addition, we observed that intersubband transitions in samples with superlattice barriers degrade faster than those transitions in samples with bulk barriers as the irradiation dose is increased.

Two multiple quantum well structures used in the present study were grown by the molecular-beam epitaxy technique on a semi-insulating GaAs substrate with 0.5 μm thick GaAs buffer layer and ~200 A thick GaAs cap layer. The structures of the two wafers are shown in table I. The barriers of the wafer labeled "B" are made of 5 periods AlGaAs/GaAs superlattices. While the barrier of the wafer labeled "A" is bulk AlGaAs. The word "*bulk*" is used here to indicate that the barrier is not a superlattice. The well regions were Si-doped {[Si]=$2x10^{18}$ cm^{-3}}. Several samples were cut and irradiated with different doses of 1 MeV protons beam. The infrared absorption spectra were recorded at the Brewster's angel of GaAs (73°) from the normal using a BOMEM Fourier-transform interferometer in conjunction with a continuous flow cryostat. The temperature was controlled within ±1.0 K and the spectra were measured at either 77 K or 300 K.

Table I: Structures of the wafers used in the present study. All wafers were Si-doped in the well {[Si] = $2.0x10^{18}cm^{-3}$}. The barrier materials of wafer "B" is made of AlGaAs/GaAs superlattice.

Wafer	*A*	*B*
Well thickness (Å)	*75*	*105*
GaAs		
Barrier material	*$Al_{0.3}Ga_{0.7}As$*	*$Al_{0.4}Ga_{0.6}As$-GaAs*
Barrier Thickness (Å)	*100*	*105 - 35*
Barrier period	*----*	*5*
MQWs period	*50*	*50*

A few spectra of the intersubband transitions in samples cut from wafer "A" and irradiated with different proton beam doses are shown in Fig. 6. The spectra were measured at 77 K. Spectrum (a) is obtained for a sample that received a dose of $2.0x10^{12}$ cm^{-2}, which is identical to the spectrum of the unirradiated samples. This indicates that the above dose did not produce significant atomic displacement damage to cause any change in the spectrum. As the dose is increased, the intensity of the spectra is reduced. However, the intersubband transitions remain observable in samples irradiated with doses as high as $5.0x10^{14}$ cm^{-2}.

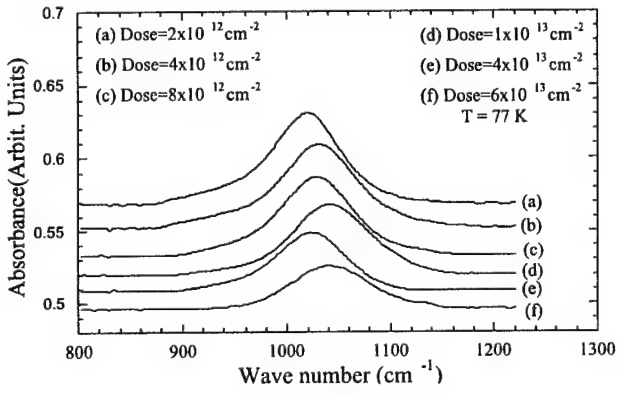

Fig. 6. A few optical absorbance spectra measured at 77 K of intersubband transitions in GaAs/AlGaAs MQW samples cut from wafer "A". The samples received different proton irradiation doses.

The peak position energy of the spectra in this figure is shifted. It was determined by measuring the spectra of the samples before and after irradiation that this shift is due to the non-uniformity of the wafer. It was found that the peak position energies in samples cut near the rim of the wafer are higher than those in samples cut from the center of the wafer.

In Fig. 7, we plotted a few spectra, measured at 77 K, of intersubband transitions in samples cut from wafer "B" and irradiated with different doses. By inspecting this figure, we noted that a dose of $1.0x10^{12}$ cm^{-2} causes some change in the total integrated area as compared the control (unirradiated) sample. We also observed that samples cut from wafer "B" and irradiated with doses higher than $3.0x10^{13}$ cm^{-2}, do not exhibit intersubband transitions. Spectrum (f) in this figure was obtained for a sample irradiated with $3.0x10^{13}$ cm^{-2}. The intersubband transition in this sample is still observable. However, upon increasing the sample's temperature from 77 K to 300 K, we observed two peaks in the spectrum. The results are shown in Fig. 7 where two peaks observed in the spectrum measured at room temperature. The results in this figure could be explained as follows. The structure of wafer "B" was designed such that two bound electronic energy levels (ground and excited states) exist in the well. The excited state is resonant in the miniband that is formed due the superlattice barrier. This miniband consists of five close energy levels. Proton irradiation causes atomic displacement. With a proton beam dose of $3.0x10^{14}$ cm^{-2}, the damage is significant enough to alter the interfaces so that the energy levels and the miniband in the quantum well structures are shifted. Hence, the excited state in the quantum well is no longer resonant in the miniband. The two peaks in Fig. 7 (a) are thus due to electronic transitions from the ground state in the quantum wells to the first excited state and to the miniband. This plausible explanation is supported by two reasons.

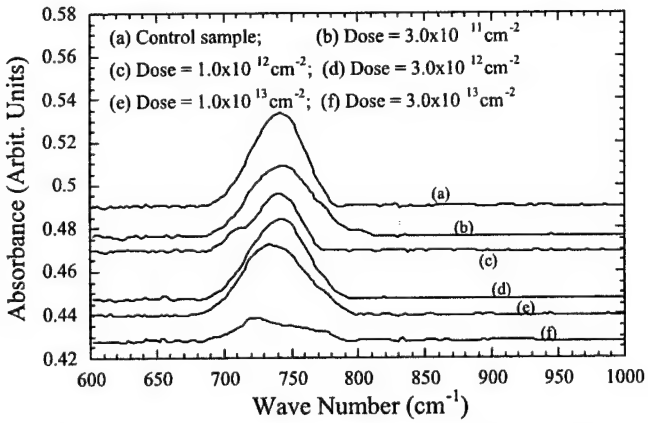

Fig. 7. A few optical absorbance spectra measured at 77 K of intersubband transitions in GaAs/(AlGaAs-GaAs) MQW samples cut from wafer "B". The samples received different proton irradiation doses. The barrier (AlGaAs-GaAs) is a 5 period superlattice.

First, the two peaks in Fig. 8 (a) were not observed in heavily irradiated samples cut from wafer "A", which does not contain a miniband in its structure. Second, as the temperature is lowered from 300 K to 77 K, the separation between the two peaks is decreased. This indicates that the separation between the excited state and the miniband

is decreased as the temperature is decreased. Similar behavior is observed in unirradiated samples designed such that the excited state is not resonant in the miniband.

Another interesting observation is seen in Fig. 8. It is noted that the total integrated area of the two peaks in spectrum (a) is decreased as the temperature is lowered from room temperature to 77 K. Similar behavior is observed in heavily electron irradiated samples. This effect is designated as a negative persistent temperature effect. It was explained as being due to the presence of irradiation induced defects. These defects trap some of the electrons in the quantum wells (two-dimensional electron gas) as the temperature is lowered. But when the temperature is increased, the electrons are released back to the quantum wells.

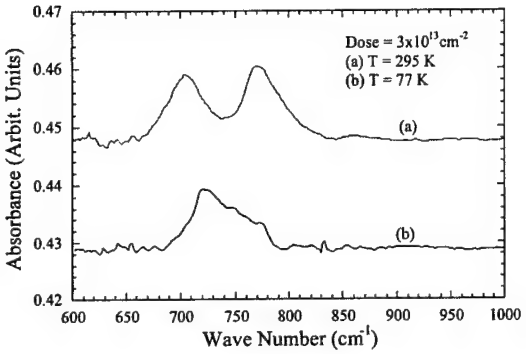

Fig. 8. Two spectra of intersubband transition in a GaAs/(AlGaAs-GaAs) measured at 77 K and 300 K for a sample cut from wafer "B" and irradiated with a dose of $3x10^{13}$ cm^{-2}. Spectrum (b) is the same as spectrum (f) in Fig. 7.

The total integrated areas, measured at 77 K, of the intersubband transitions spectra were studied as a function of proton irradiation dose. The results are shown in Fig. 8. The open squares in this figure represent the total integrated area obtained for irradiated samples that were cut from wafer "A". Integrated areas of the irradiated samples cut from wafer "B" are presented by the solid squares. The data in this figure were fitted with the following expression:

$$I = I_0 \, Exp(-\delta d), \qquad (1)$$

Where I is the total integrated area, I_0 is a fitting parameter but its value is close to the total integrated area of the unirradiated samples, δ is a second fitting parameter, and d is the irradiation dose. The fitting results are shown as solid lines in Fig. 9 for both samples cut from wafers "A" and "B".

The δ values obtained from the fitting procedure are 0.014 and 0.038 for the samples cut from wafers "A" and "B", respectively. These values indicate that the samples with superlattice barriers degrade at a faster rate as compared to samples with bulk barrier as the irradiation dose is increased. The above difference in the δ values can be explained as follows. The structure of wafer "B" contains AlGaAs/GaAs superlattice barriers, which means that the number of interfaces is much larger as compared to the structure of Wafer "A". The proton irradiation produce atomic displacement damage including point and complex defects such as antisites, interstitials and vacancies. These defects play a major role on the quality of interfaces between the epitaxial layers. Hence,

samples with smaller numbers of interfaces can withstand higher proton irradiation doses as shown for samples cut from Wafer "A". The high δ value in samples with superlattice barriers was also confirmed in another set of MQW samples cut from a wafer with a structure of 59 Å GaAs well and a barrier of 5 periods 59Å $Al_{0.4}Ga_{0.6}As$/29Å GaAs. Additional measurements may be needed to role out the idea of the faster degradation as being due to the longer absorption wavelength.

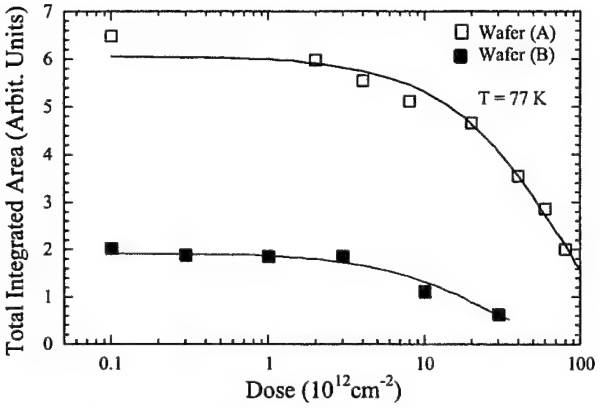

Fig. 9. Total integrated area of the intersubband transitions measured for samples cut from wafers "A" (open squares) and "B" (closed squares) as a function proton irradiation dose. The solid lines are the results of fitting the data using Eq. (1) where I_0 and δ are fitting parameters.

The results in this section describe the behavior of the optical absorption spectra of the intersubband transitions in GaAs/AlGaAs multiple quantum wells under the influence of 1 MeV proton irradiation and doses ranging between $1.0x10^{12}$ and $5.0x10^{14}$ cm^{-2}. It is observed that the total integrated area of the intersubband transitions are dramatically decreased as the irradiation dose is increased. This reduction was interpreted as being due to the trapping of the two-dimensional electrons gas by the irradiation induced-defects. The total integrated areas of the intersubband transitions were studied as a function of irradiation doses for samples cut from wafers with structures containing either balk or superlattice barriers. The results reveal that the intersubband transitions in samples with superlattice barriers degrade at a faster rate as compared to those transitions in samples with bulk barriers.

6. Thermal Annealing Recovery of Intersubband Transitions in Proton-Irradiated GaAs/AlGaAs Multiple Quantum Wells

In this section, we report on the thermal recovery of depleted intersubband transitions in proton irradiated GaAs/AlGaAs multiple quantum well samples. The intersubband transitions were measured before and after proton irradiation and it was observed that the intersubband transitions were completely washed out in samples irradiated with 1 MeV protons and doses higher than $4x10^{14}$cm^{-2}. Upon isochronal thermal annealing, these transitions were observed to recover at annealing temperatures (T_a) as low as 250 °C in samples that received low irradiation doses. Both the total integrated areas and the peak position energies of the intersubband transitions in irradiated samples and in one-reference sample were measured as a function of T_a. The T_a at which the recovery occurred was found to depend on the protons irradiation dose.

This observation will be explained in terms of irradiation induced-defect species, which trap the two-dimensional electron gas. The behavior of the total integrated areas and the peak position energies of the intersubband transitions will be explained in terms of energy level shifts due to interdifussion.

Two multiple quantum well structures used in the present study were grown by the molecular-beam epitaxy technique on a semi-insulating GaAs substrate with a 0.5 μm thick GaAs buffer layer and a ~200 Å thick GaAs cap layer. The structures of the two wafers are shown in table II. The barriers of the wafer labeled "A" are bulk AlGaAs. While the barriers of the wafer labeled "B" are made of 5 periods AlGaAs/GaAs superlattices. The well regions were Si-doped {[Si]=$2x10^{18}$ cm^{-3}}. Several samples were cut and irradiated with different doses of 1 MeV proton beams. The infrared absorption spectra were recorded at the Brewster's angle of GaAs (73°) from the normal using a BOMEM Fourier-transform interferometer in conjunction with a continuous flow cryostat. The temperature was controlled within ±1.0 K and the spectra were measured at either 77K or 300K. Furnace thermal annealing was performed in a continuous flow of nitrogen gas in the T_a range of 200 – 800 °C. The annealing time at each temperature was 15 minutes.

Table II: Structures of the wafers used in the present study. All wafers were Si-doped in the well {[Si] = $2.0x10^{18}cm^{-3}$}. The barrier material of wafer "B" is made of AlGaAs/GaAs superlattice.

Wafer	A	B
Well thickness (Å) GaAs	75	59
Barrier material	$Al_{0.3}Ga_{0.7}As$	$Al_{0.4}Ga_{0.6}As$ - GaAs
Barrier Thickness (Å)	100	59 - 29
Barrier period	----	5
MQWs period	50	50

A few absorbance spectra of an intersubband transition in a sample cut from wafer "A" were measured at 77 K and plotted in Fig. 10. Spectrum (a) was obtained for the sample before any proton irradiation or thermal annealing. Spectrum (b) corresponds to the same sample after it was irradiated with a dose of $4x10^{14}cm^{-2}$. It is clear from this figure that the intersubband transition was completely depleted. Spectra (c) and (d) were obtained after annealing the irradiated sample at T_a =400 and 600 °C, respectively. It is obvious that the intersubband transition is recovered by thermal annealing. The total integrated area of the intersubband transition in spectrum (d), which is the spectrum obtained for the irradiated sample and after thermal annealing at 600 °C, is about 80% of that of spectrum (a).

It is observed that a partial recovery of the intersubband transition in the sample cut from wafer "A" and irradiated with a dose of $4x10^{14}cm^{-2}$ is achieved at T_a as low as 250 °C. However, the thermal annealing behavior of the intersubband transition is quite different in a sample irradiated with a dose of $2x10^{16}cm^{-2}$. The results are shown in Fig. 11. Spectrum (a) is the absorbance of the intersubband transition in the as grown sample

(reference sample) cut from wafer "B". Spectrum (b) is obtained for a sample cut from the same wafer which was irradiated with a dose of $2x10^{16}cm^{-2}$. The signature of the intersubband transition in this spectrum is absent. Thermal annealing recovery of the intersubband transition in the irradiated sample is observed at T_a above 625 °C. For comparison, spectrum (c) in Fig. 11 is plotted for the irradiated sample after it was annealing at 725 °C.

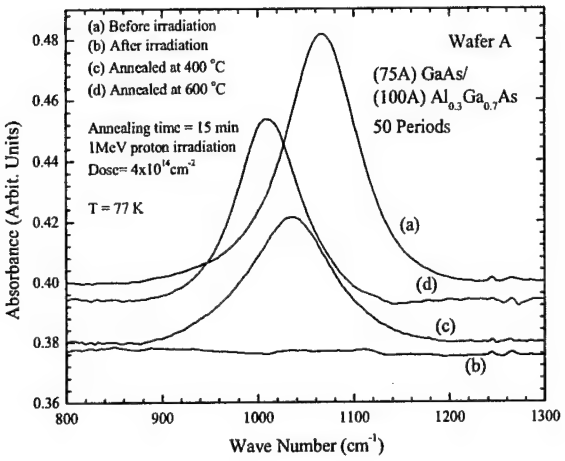

Fig. 10. Absorbance spectra of intersubband transitions measured at T = 77 K for a sample cut from wafer "A." Spectrum (a) was obtained before thermal annealing and before proton irradiation. Spectrum (b) was obtained for the same sample after it was irradiated with dose of $4x10^{14}cm^{-2}$. Spectra (c) and (d) were measured after irradiation and after thermal annealing the sample at 400 and 600 °C, respectively.

To better understand the processes associated with the irradiation and thermal annealing effects on GaAs/AlGaAs multiple quantum wells, we tracked the total integrated areas of the intersubband transitions as a function of annealing temperatures for three samples as shown in Fig. 12. First, a reference sample (unirradiated) cut from wafer "B" was annealed and the results are presented by the solid squares in this figure. About 10% reduction in the total integrated area was observed in this sample as T_a is changed from 350 °C to 700 °C. Then the area is reduced to about 50% after the sample is annealed at T_a = 775 °C. On the other hand, the integrated area of the intersubband transition in a sample cut from wafer "B" and irradiated with a dose of $2x10^{16}cm^{-2}$ remains zero until T_a reached 650 °C (see solid circles). A total recovery of 50% is observed at T_a = 750 °C for the intersubband transition in the irradiated sample as compared to the that of the unirradiated sample, which were both cut from wafer "B". On the other hand, the thermal annealing recovery of a sample cut from wafer "A" and irradiate with $4x10^{14}cm^{-2}$ occurred at T_a as low as 250 °C (Fig. 12 open squares) and reached about 80% at T_a = 600 °C.

The thermal annealing recovery of intersubband transitions presented in Figs. 10-12 can be explained as follows. Antisites, interstitials, and vacancies are the primary point defects introduced by energetic charged particle irradiation, such as protons and electrons, in gallium arsenide and presumably AlGaAs as well. These point defects may form more complex defects as the irradiation dose is increased, but both irradiation induced-point and -complex defects produce energy levels in the band gap that act as traps for both electrons and holes. Thus, 1 MeV protons irradiation doses of $4x10^{14}$ and $2x10^{16}cm^{-2}$ produce defect energy levels in the band gap. These defects then trap the

two-dimensional electron gas formed in the GaAs wells causing a reduction in the total integrated areas of the intersubband transitions, which is directly proportional to the electron density in the quantum wells[9]. It was noted previously that the intersubband transitions were depleted in samples irradiated with proton doses as low as $1x10^{14}cm^{-2}$. Proton irradiation induced defects, in particular vacancies and antisites related defects,

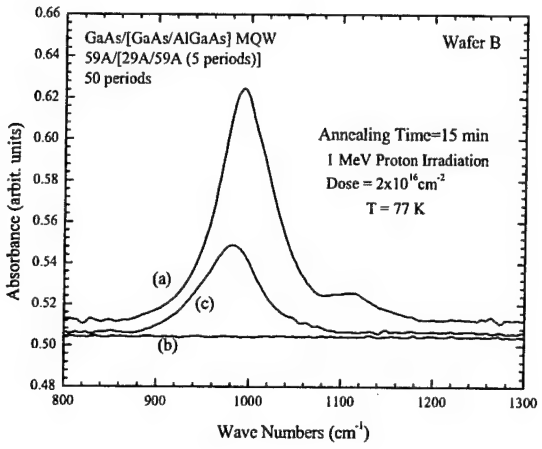

Fig. 11. Absorbance spectra of intersubband transitions measured at T = 77 K for samples cut from wafer "B." Spectrum (a) was obtained for unirradiated sample before thermal annealing. Spectrum (b) was obtained for another sample after it was irradiated with a dose of $2x10^{16}cm^{-2}$. Spectrum (c) was measured for the irradiated sample and after thermal annealing at 725 °C.

can be easily annealed out. Such defects usually dominate the lower dose irradiated samples and demonstrated by the fact that the intersubband transitions are partially recovered in such irradiated samples after thermal annealing. It is worth mentioning here that the sample with lower irradiation dose (see Fig. 10 and open squares in Fig. 12) shows that the intersubband transition is thermally recovered (partially) at much lower temperature as compared to the sample that received a higher irradiation dose (see Fig. 11 and the solid circles in Fig. 12). This observation indicates that the electron traps in samples with the lower irradiation doses are dominated by vacancies and interstitials related defects, which are well known[5,6,10] to anneal out at temperatures as low as 200-250 °C. Hence, the electrons are released back to the quantum well causing the partial thermal recovery of the intersubband transition. Higher irradiation doses on the other hand, produce thermally stable defects such as arsenic antisites and antisite related traps, which can be annealed out at temperatures higher than 500 °C. It is clear from Fig. 12 (see solid circles) that the intersubband transition in the sample irradiated with a dose of $2x10^{16}cm^{-2}$ starts recovery at $T_a > 600$ °C in support of the premise that antisite related defects are responsible for trapping of the two-dimensional electron gas in the heavily irradiated samples.

Proton irradiation and thermal annealing also have detrimental effects on the quantum well interfaces. When thin layers of semiconductor quantum well structures are grown

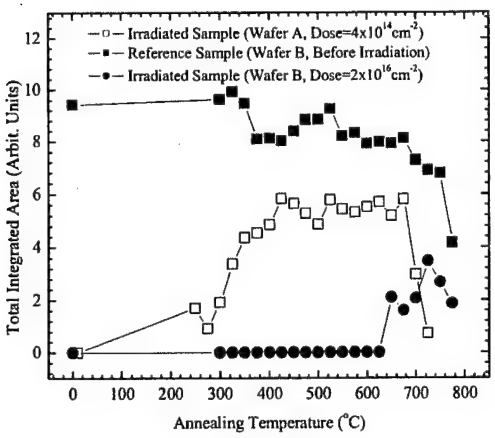

Fig. 12. Total integrated area of the intersubband transitions measured at T = 77 K for a reference sample cut from wafer "B" (solid squares), a sample cut from wafer "A" and irradiated with a dose of $4x10^{14}cm^{-2}$ (open squares), and a sample cut from wafer "B" and irradiated with a dose of $2x10^{16}cm^{-2}$ (solid circles).

epitaxially, an interdifussion or reordering of the atoms at the interfaces occurs, causing a change in the composition profile of the structures. This intermixing can be accelerated by impurities and dopants or by thermal annealing. As the quantum well profile is converted from a rectangular shape to a more parabolic shape due to intermixing, the energy levels in the conduction quantum wells are shifted upwards with the ground state being shifted more than the first excited state. Hence, a reduction of the peak position energy of the intersubband transition in the GaAs/AlGaAs multiple quantum wells can be observed. This is demonstrated in Fig. 13 where the peak position energy of the intersubband transitions in two samples is plotted as a function of annealing temperature. The solid squares were obtained for the reference sample cut from wafer "B". The open squares represent the results obtained for a sample cut from wafer "A" and irradiated with a dose of $4x10^{14}cm^{-2}$. We observed a small shift in the peak position energy in the reference sample as T_a is changed from 300 to 700 °C.

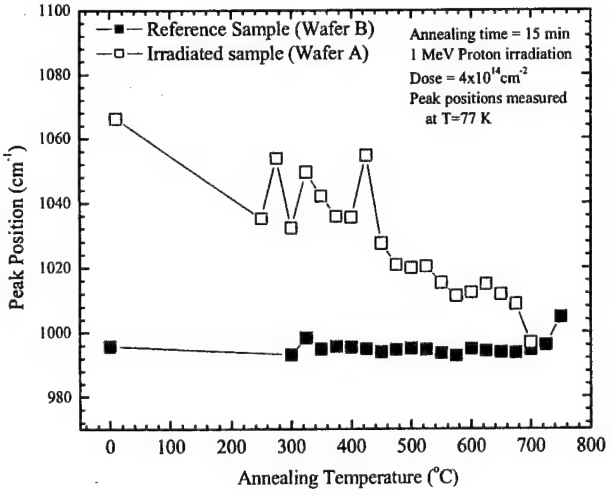

Fig. 13. The peak position energies of intersubband transitions in two samples measured at T = 77 K as a function of the annealing temperature. The solid squares represent the results obtained for the reference sample cut from wafer "B" and the open squares represents the results obtained for the sample that was cut from wafer "A" and irradiated with a dose of $4x10^{14}\ cm^{-2}$.

On the other hand, the results obtained for the irradiated sample show a large decrease in the peak position energy as T_a is changed from 250 to 700 °C. The slight increase of the peak position energy of the reference sample above 700 °C perhaps due to the shift of the excited state to the continuum as the intermixing processes become dominant at $T_a > 700$ °C. Further study is needed to provide a more comprehensive understanding of this behavior since it was observed in many samples that we tested. It is clear from Fig. 13 that the intermixing process is more prominent in the irradiated sample as judged by the large decrease in the peak position energy of the intersubband transition, which leads us to conclude that irradiation induced-defects can also accelerate disordering at the quantum well interfaces.

The thermal annealing recovery of intersubband transitions in proton irradiated GaAs/AlGaAs multiple quantum wells is reported in this section. It was observed that thermal annealing reduces the intensity of the intersubband transitions in as-grown and unirradiated samples. The depleted intersubband transitions in heavily irradiated samples were observed to recover as the annealing temperature is increased. Is was also observed that the annealing temperature threshold at which the initial recovery of the intersubband transition depends on the irradiation dose. The results are explained in terms of irradiation-induced vacancy, interstitial, and antisite defects, which trap the two-dimensional electron gas in the quantum wells. As these traps are annealed out, the electrons are released back to the wells causing the observed recovery. Intermixing and disordering processes were invoked to explain the variation of the peak position energies of the intersubband transitions as a function of thermal annealing temperature.

6. He^+-ion irradiation effect on intersubband transitions in GaAs/AlGaAs multiple quantum wells.

In this section, we report on 3 MeV He^+-ion irradiation effects on the intersubband transitions in GaAs/AlGaAs multiple quantum well samples. The intersubband transitions were measured before and after He^+-ion irradiation and it was observed that the intersubband transitions were completely washed out in samples irradiated with H^+-ion fluences as low as $1x10^{14}cm^{-2}$. Upon isochronal thermal annealing, these transitions were observed to partially recover at annealing temperatures (T_a) as low as 350 °C in samples that received lower irradiation doses. But thermal annealing does not seems to cause any recovery in samples irradiated with doses higher than $4x10^{14}$ cm^{-2}. The total integrated areas of the intersubband transitions in irradiated samples and in one-reference sample were measured as a function of T_a. The T_a at which the thermal annealing recovery of the depleted intersubband transition occurred was found to increase as the irradiation dose is increased.

A multiple quantum well structure used in the present study was grown by the molecular-beam epitaxy technique on a semi-insulating GaAs substrate with a 0.5 μm thick GaAs buffer layer and a ~200 Å thick GaAs cap layer. The structure is made of 50 periods of 75 Å thick GaAs well and 100 Å $Al_{0.3}Ga_{0.7}As$ barrier. The middle 50 Å of the GaAs well region was Si-doped {[Si]=$1x10^{18}$ cm^{-3}}. Numerous samples were cut from the same wafer and irradiated with different doses of 3 MeV He^+-ion generated in a

tandem Van de Graaf accelerator, and incident at 7° from the surface normal in order to reduce ion-channeling effects.

The infrared absorption spectra were recorded at the Brewster's angle of GaAs (73°) from the normal using a BOMEM Fourier-transform interferometer in conjunction with a continuous flow cryostat. The temperature was controlled within ±1.0 K and the spectra were measured at either 77K or 300K. Furnace isochronal thermal annealing was performed in a continuous flow of nitrogen gas in the T_a range of 200 – 800 °C. The samples were sandwiched between semi-insulating wafers during annealing to reduce the loss of As. The annealing time at each temperature was 15 minutes.

Absorbance spectra, measured at 77 K, of intersubband transitions in several samples cut from the same wafer described above and irradiated with different doses are plotted in Fig. 14. It is clear from this figure that the intensity of the intersubband transition is decreased as the dose is increased. It is also observed that the peak position of the intersubband transition is shifted toward lower energy in spectra (b) and (c). This can be explained in terms of reduction of the two-dimensional electron gas (2DEG) density in the quantum wells due to trapping by radiation-induced defects. The reduction of the 2DEG density causes a decrease of many-body effects, which lead to this type of shift. The peak position of the spectra (d) and (e) were shifted to higher energy. This is found to be due to the non-uniformity of the wafer. We noted that samples cut near the rim of the wafer exhibit higher peak position energy before irradiation. But their peak position energies were shifted toward lower energy after irradiation. Spectrum (f) was taken for a sample that was irradiated with a dose of $1x10^{14}$ cm^{-2}. It is clear that this dose causes a complete depletion of the intersubband transition.

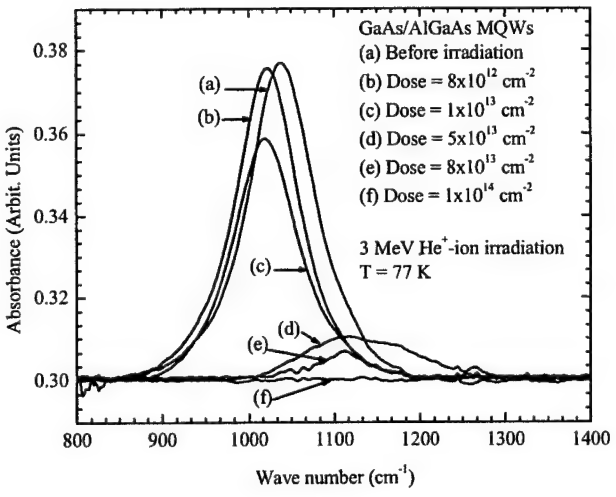

Fig. 14. Absorbance spectra of intersubband transitions in unirradiated [spectrum (a)] and 3 MeV He^+-ion irradiated GaAs/AlGaAs MQWs measured at T = 77K. The doses are (b) $8x10^{12}$ cm^{-2}, (c) $1x10^{13}$ cm^{-2}, (d) $5x10^{13}$ cm^{-2}, (e) $8x10^{13}$ cm^{-2}, and (f) $1x10^{14}$ cm^{-2}.

Isochronal thermal annealing was performed for a sample irradiated with a dose of $5x10^{13}cm^{-2}$ and the results are shown in Fig. 15. Spectra (a) and (b) were measured before and after irradiation, respectively. Spectra (c), (d), and (e) were measured after irradiation and after isochronal thermal annealing for 15 min at 325, 450, and 625 °C, respectively. All spectra were recorded at 77 K. The partial thermal recovery of the

intersubband transitions can be explained as follows. 3 MeV He^+ - ion irradiation produced defects that can trap the 2DEG. These traps must be related to vacancies, interstitials and antisites. The radiation-induced defects are annealed out, hence releasing the electrons back to the quantum well, which causes the partial recovery of the intersubband transition.

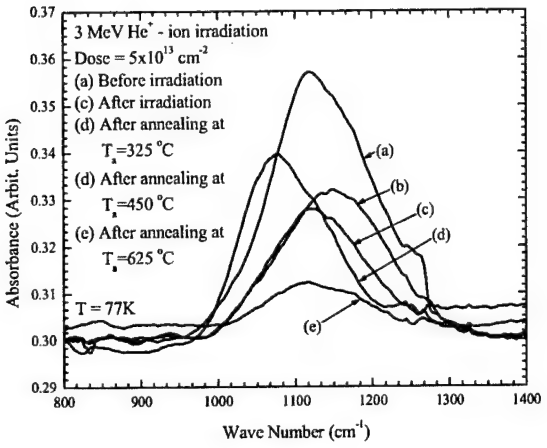

Fig. 15. Thermal annealing recovery of intersubband transitions in He^+-ion irradiated GaAs/AlGaAs MQW sample. The irradiation dose was $5x10^{13}$ cm^{-2} and the annealing time was 15 min at temperature.

A complete recovery of the intersubband transition has not been reached. This is because other effects such as intermixing and interdifussion are introduced as the thermal annealing temperature is raised above 600 °C. To illustrate this finding, we tracked the total integrated areas of the intersubband transitions in irradiated and unirradiated samples as a function of annealing temperature. The results are shown in Fig. 16. The solid squares represents the data obtained for the control sample. The total integrated area of the intersubband transition in the control sample (see squares) is slowly increased as the annealing temperature is increase from 200 to 675 °C. This integrated area is dramatically decreased as the annealing temperature is increased above 700 °C. The same behavior is observed for the samples irradiated with doses of $5x10^{13}$ cm^{-2} (circles), $8x10^{13}$ cm^{-2} (diamonds), and $1x10^{14}$ cm^{-2} (triangles). However, it is noted from this figure that the magnitude of the thermal annealing recovery of the intersubband transition in the irradiated samples is decreased as the irradiation dose is increased. For example, the integrated area measured after annealing the $1x10^{14}$ cm^{-2} irradiated sample (see triangles) at 400 °C is lower than that of the sample irradiated with a dose of $5x10^{13}$ cm^{-2} (see circles). Additionally, the annealing temperature threshold at which the recovery started is also increased as the irradiation dose is increased. This could be explained as follows. Lower irradiation doses produce vacancy and interstitial related point defects that are well known to anneal out at temperatures as low as 200-250 °C. Hence, the electrons are released back to the quantum well causing the partial thermal recovery of the intersubband transition. Higher irradiation doses on the other hand, produce more thermally stable defects such as arsenic antisites and antisite related traps, which can be annealed out at temperatures higher than 500 °C causing the slower thermal annealing recovery since the annealing of traps is accompanied by the release of the electrons to the quantum wells.

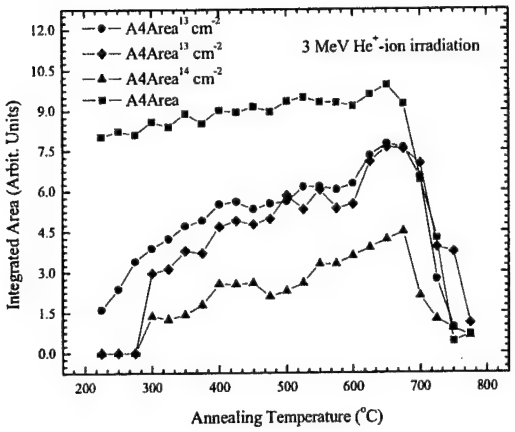

Fig. 16. The total integrated area of the intersubband transitions in the control (squares) and irradiated GaAs/AlGaAs MQW samples (circles, diamonds and triangles) obtained as a function of annealing temperature. The annealing time was 15 min at each temperature.

He^+-ion irradiation and thermal annealing to temperature over 600 °C also have detrimental effects on the quantum well interfaces. When thin layers of semiconductor quantum well structures are grown epitaxially, an interdifussion or reordering of the atoms at the interfaces occurs, causing a change in the composition profile of the structures. This intermixing can be accelerated by impurities and dopants or by thermal annealing. As the quantum well profile is converted from a rectangular shape to a more parabolic shape due to intermixing, the energy levels in the conduction quantum wells are shifted upwards with the ground state being shifted more than the first excited state. Hence, a reduction of the peak position energy of the intersubband transition in the GaAs/AlGaAs multiple quantum wells can be observed. When the annealing temperature is sufficiently high, the excited states may be pushed out of the quantum wells causing a reduction in the quantum confinement and in the oscillator strength of the transitions. Hence, one expect to see a drastic reduction in the intensity of the intersubband transitions as shown in Fig. 16 for all samples, including the control sample, at annealing temperature above 675 °C.

Finally, the intersubband transition is completely depleted in samples irradiated with 3 MeV He^+-ion with doses as low as $1x10^{14}$ cm^{-2}. These doses are much smaller than the proton and electron doses that cause a complete depletion of the intersubband transition. As expected, this is due to the fact that He^+ - ion are more massive than electrons and protons and therefore causes more extensive damage to the quantum structures and interfaces.

In this section, 3 MeV He^+-ion irradiation effect on intersubband transitions in GaAs/AlGaAs multiple quantum wells is investigated. A complete depletion of the intersubband transition is observed in samples irradiated with doses as low as $1x10^{14}cm^{-2}$. This dose is lower than those of proton and electrons that produced the same effect due to the fact that He^+ - ion are more massive and hence cause more damage to the quantum structures and their interfaces. Isochronal thermal annealing of intersubband transitions in irradiated samples was performed and partial recovery is reached in samples irradiated with doses smaller than $4x10^{14}$ cm^{-2}. Samples irradiated with higher doses do not show thermal recovery due to the catastrophic irradiation-induced damage. The total integrated

area of the intersubband transition was also investigated in irradiated samples as a function of thermal annealing temperature. The behavior of the thermal annealing recovery of the intersubband transition was found to depend on the irradiation dose.

7. Nitrogen Vacancy in Proton-Irradiated $Al_xGa_{1-x}N$

III-nitride semiconductors have been one of the most investigated classes of materials in recent years due to their optoelectronic applications in the ultraviolet and visible spectral regions. Since the optical and electronic qualities of a semiconductor are highly influenced by the nature of impurities, dopants and native defects, it is thus very important to understand the properties of these defects. As grown GaN is n-type and the n-type conductivity has been associated with the nitrogen vacancy. In this section, we report on the direct observation of nitrogen vacancy (V_N) in proton irradiated AlGaN thin films using the optical absorption technique. The present optical absorption measurements of the V_N energy level indicate that this energy level is above and below the conduction band minimum of GaN and AlN, respectively. A shoulder was also observed in the spectrum suggesting that there are more than one optically active energy level associated with the V_N. Additionally, the present results show that the V_N energy level emerges out of the conduction band into the fundamental bandgap at $x = 0.45$. A comparison between the present results and the previously reported theoretical calculations will be presented.

The $Al_xGa_{1-x}N$ thin films of thickness 1 μm or less were grown by metalorganic chemical vapor deposition technique on sapphire substrates. Each sample investigated here was irradiated with the following proton doses: 10 keV ($3.5x10^{15}$ cm^{-2}), 20 keV ($3.8x10^{15}$ cm^{-2}), 30 keV ($4.4x10^{15}$ cm^{-2}), 50 keV ($6.0x10^{15}$ cm^{-2}), 70 keV ($6.3x10^{15}$ cm^{-2}), and 100 keV ($9.7x10^{15}$ cm^{-2}). This irradiation scheme was chosen to produce a constant profile of ~$4.0x10^{20}$ proton/cm^{-2} in the depth range of 0 – 0.8 μm.

During each irradiation step, the ion-beam flux was kept relatively low (<$7x10^{12}$ cm^{-2} s^{-1}), which produce a negligible ion-beam heating effect. Hence, the samples' temperature remains around room temperature during irradiation to avoid annealing the induced vacancies. Nitrogen vacancies were not observed in samples irradiated with 1 MeV protons since the sample temperature was increased above 160 °C during irradiation. The optical absorption spectra were collected using a Varian Cary 500 spectrometer in conjunction with a closed-cycle refrigerator. Several $Al_xGa_{1-x}N$ samples with different Al mole fractions including binary compounds ($x = 0$ and 1) samples were irradiated with proton. The optical absorption spectra were measure at 10 K before and after irradiation. A few spectra are shown in Fig. 17 for four samples that illustrate the V_N energy level as the *Al* mole fraction (*x)* is changed from 0.35 to 1. In Fig 17.(a) the spectrum of the sample after irradiation is red-shifted but a peak was not observed since the V_N energy level is still resonant in the conduction band. In Fig. 1(b) the spectrum of the irradiated sample exhibit a shoulder at 4.11 eV. However, upon irradiating an $Al_{0.6}Ga_{0.4}N$ sample, the spectrum [Fig. 17 (c)] shows a peak at 4.610 eV and shoulder at 4.220 eV. This sample clearly demonstrates that the V_N energy level is emerged from the conduction band into the fundamental band gap. It is clear from these spectra that the V_N energy level can be observed in samples where the band edge absorption is higher than the V_N absorption band. Stronger evidence of the presence of the V_N energy level is

shown in the spectrum of the AlN sample in Fig. 17 (d), where the band gap is 6.28 eV. The peak observed in spectrum (2) in Fig. 17 (d) is broad and it appears to be composed of two peaks. In fact, when a baseline correction was made for spectrum (2) in Fig. 1(c), the spectrum shape is found to be identical to that of spectrum (2) in Fig. 17 (d).
It is found that the total integrated area of the V_N absorption band in samples with $0.50 \leq x \leq 0.61$ is approximately twice as large as that of V_N absorption band in AlN samples. This suggests that the production rate of the V_N in the proton irradiated samples is decreased as the *Al* mole fraction is increased. Based on this finding, we estimated the

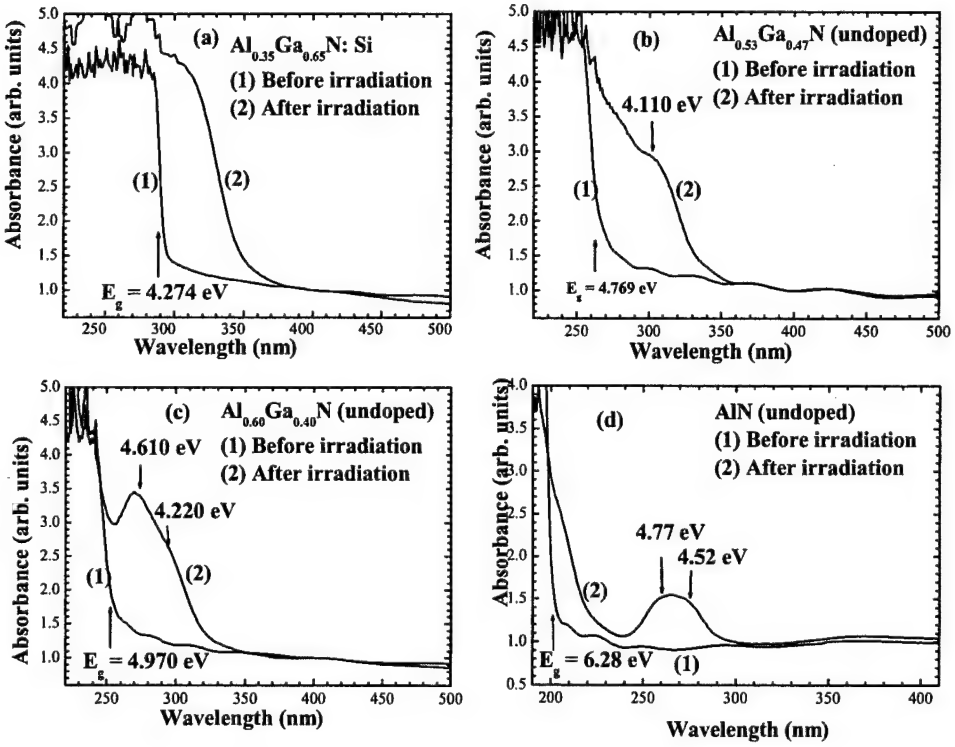

Fig. 17. Optical absorption spectra of $Al_xGa_{1-x}N$ samples measured at 10 K before and after proton irradiation, where x is (a) 0.35, (b) 0.53, (c) 0.60, and (d) 1.0. The absorption band observed below the band edge is assigned to the nitrogen vacancy.

V_N energy level in lower *Al* mole fraction samples by using the following procedure. The threshold energy of the V_N absorption band was measured for all samples with $0 \leq x \leq 1$. Then the peak position energy of the V_N absorption band was measured for the samples with $x \geq 0.55$. The difference between the peak position and the threshold energies (ΔE) was then calculated for the samples with $x \geq 0.55$ and fitted with a linear equation. The results is found to be ΔE (nm) = 99 – 65 x. Finally, the peak position was estimated for

the samples where the V_N energy level is still above the conduction band minimum by subtracting ΔE from the threshold energy. Again, the threshold energy was found to be below the conduction band minimum for all samples including GaN. The nitrogen vacancy energy level obtained here is plotted along the conduction and valence bands of AlGaN in Fig. 18. Solid squares are the measured (estimated) V_N peak position energy for the irradiated samples with $x \geq 0.55$ ($x < 0.55$). Linear fitting of the V_N peak position energy gives

$$E(V_N) = 4.23 + 0.67\,x \text{ (eV)}, \tag{2}$$

where $E(V_N)$ is the nitrogen vacancy energy level. This linear relationship is shown as dashed line in Fig. 18. The valence band was taken as the reference energy (0.0 eV) and the conduction band was obtained from the optical absorption spectra measured in several unirradiated samples with different *Al* mole fractions. The conduction band minimum was fitted with a nonlinear equation and the result is shown in the following expression:

$$E_g(x) = 3.495\,(1 - x) + 6.28\,x - 0.85\,x\,(1 - x). \tag{3}$$

It is clear from Fig. 18 that $E(V_N)$ resonant in the conduction band and emerges into the fundamental band gap at $x \simeq 0.45$.

Most theoretical calculations of point defects in III-nitride semiconductors were performed for binary compounds. The general consensus is that V_N has two states. In GaN there are s-like (A_1) states that are resonant in the valence band and p-like (T_2) states, which are resonant in the conduction band. Additionally, the p-like state is split into a singlet and doublet. It was estimated that the singlet state is about 0.8 eV above the bottom of the conduction band or 4.25 eV above the valence band assuming that the GaN band gap is 3.45 eV. This calculated value is in good agreement with the estimated V_N energy level value of 4.08 eV obtained from the present measurements and with the value of 4.23 eV obtained from Eq. (1). The present measurements as shown in Fig. 17 (d) clearly demonstrate that T_2 state is in fact exists in the fundamental band gap.

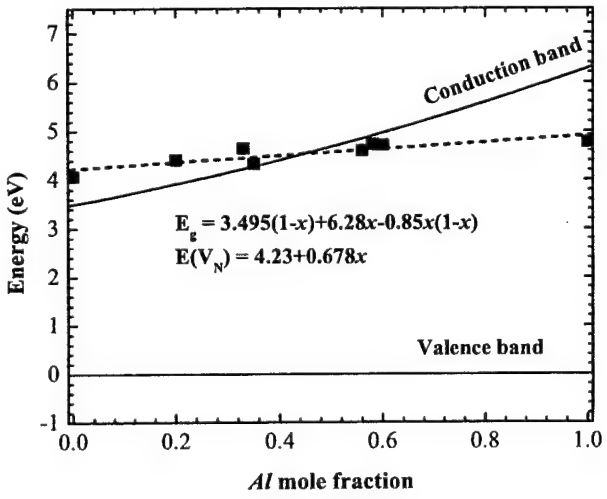

Fig. 18. The peak position energy of the nitrogen vacancy energy level determined by the optical absorption technique is plotted as a function of the Al mole fraction (solid squares). The dashed line is a linear fit of the experimental data and presents Eq. (2). The solid lines are the valence band maximum and the conduction band minimum plots as a function of x. The conduction band minimum was plotted using Eq. (3).

Isochronal annealing was performed on the $Al_{0.6}Ga_{0.4}N$ irradiated sample shown in Fig. 17(c). The result is shown in Fig. 19. In this figure we plotted the total integrated area measured under the peak and the shoulder shown in spectrum (2) in Fig. 17 (c) as a function of annealing temperatures. The sample was annealed for 15 min at each temperature. The total integrated area is directly proportional to the density of the defect. We assumed that both the peak and the shoulder are belonging to the same defect since the isochronal annealing rate is found to be the same for both the peak and the shoulder. It is clear from this figure that the defect responsible for the absorption band with the peak and shoulder starts to anneal out at 200 °C and it is almost washed out when the annealing temperature reached 450 °C. We observed that those defects are completely annealed out when the sample is isothermally annealed for longer periods of time at temperatures as low as 400 °C. The annealing results confirmed our assumption that the irradiation-induced defect observed in the optical absorption spectra in proton irradiated.

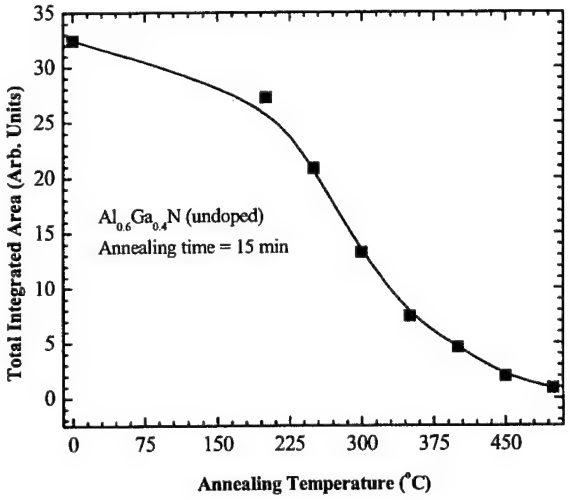

Fig. 19. The total integrated area of the nitrogen vacancy band observed in the proton irradiated $Al_{0.6}Ga_{0.4}N$ sample shown in Fig. 17(c) as a function of thermal annealing temperature. The sample was annealed for 15 min at each temperature. The solid line is drawn as a guide to the eye.

sample is indeed a nitrogen vacancy. The annealing temperature range used here (200 – 400 °C) is a typical range for annealing donor vacancies in III-V semiconductors For example, the antisites are usually annealed out at temperature higher than 600°C while interstitials and accepter vacancies are annealed at temperature lower than 150°C or even below room temperature.

In this section, we presented optical absorption spectra for the nitrogen vacancy in proton irradiated $Al_xG_{1-x}N$ samples. The results indicate that the nitrogen vacancy energy level (T_2) is resonant in the conduction band and emerges into the fundamental band gap at x~0.45. A peak and a shoulder were observed in the nitrogen vacancy absorption band and the peak position is found to be 4.77 eV in AlN. The nitrogen vacancy energy level was extrapolated to the GaN samples and found to be ~ 4.08 eV. These results were found to be in good agreement with the reported theoretical calculations of the nitrogen vacancy in both GaN and AlN materials. Isochronal thermal annealing shows that the observed absorption band that is assigned to the nitrogen vacancy starts to anneal out at

temperatures as low as 250 °C. Based on the total integrated area of the nitrogen vacancy absorption band, we additionally concluded that the production rate of the nitrogen vacancy in proton irradiated $Al_xGa_{1-x}N$ is decreased as x is increased.

8. Thermal Annealing Effect on Nitrogen Vacancy in Proton Irradiated $Al_xGa_{1-x}N$.

Since the optical and electronic qualities of a semiconductor are highly influenced by the nature of impurities, dopants and native defects, it is thus very important to understand the properties of these defects. In this section, we report on the thermal annealing behavior of an absorption band observed below the band edge in proton irradiated AlGaN samples and attributed to the nitrogen vacancy (V_N) in the previous section. The isothermal annealing is performed in the temperature range of 150 – 350 °C, which is the range that group V vacancies in III-V compound semiconductors were found to anneal out. The full width at half maximum (FWHM) of the V_N absorption band is investigated in the temperature range of 10 – 300 K. From fitting the FWHM data using the configuration coordinate model, we estimated that the broadening of the band is due to a phonon coupling with an energy of 47.8 meV. Frank-Condon shift was also estimated and found to be large enough to conclude that there is a large lattice distortion in the vicinity of the defect.

Two undoped $Al_xGa_{1-x}N$ thin films with x = 0.61 and 1.0 and of thickness 1 μm or less were grown by metalorganic chemical vapor deposition technique on sapphire substrates. Each sample investigated here was irradiated with the following proton doses: 10 keV ($3.5x10^{15}$ cm^{-2}), 20 keV ($3.8x10^{15}$ cm^{-2}), 30 keV ($4.4x10^{15}$ cm^{-2}), 50 keV ($6.0x10^{15}$ cm^{-2}), 70 keV ($6.3x10^{15}$ cm^{-2}), and 100 keV ($9.7x10^{15}$ cm^{-2}). This irradiation scheme was chosen to produce a constant profile of ~$4.0x10^{20}$ proton/cm^{-2} in the depth range of 0 – 0.8 μm. During each irradiation step, the ion-beam flux was kept relatively low (<$7x10^{12}$ cm^{-2} s^{-1}), which produce a negligible ion-beam heating effect. Hence, the samples' temperature remains around room temperature during irradiation to avoid annealing the induced vacancies. The optical absorption spectra were recorded using a Varian Cary 500 spectrometer in conjunction with a closed-cycle refrigerator, which is used to cool the samples to 10K.

The absorbance spectra for the $Al_{0.61}Ga_{0.39}N$ and AlN samples are shown in Fig. 20 (a) and (b), respectively, before and after irradiation and after thermal annealing the irradiated samples at different temperatures. The oscillations in the spectrum collected before irradiation in Fig. 20 (b) are due to the interference in the epitaxial thin film. These interference patterns are used to estimate the layer thick. From this figure we estimated the AlN thin film thickness to be 0.43 μm assuming a refractive index value of 2.2. As pointed out previously[8], the absorption band observed in both $Al_{0.61}Ga_{0.39}N$ and AlN samples is composed of a peak and a shoulder overriding the lower energy side of the peak. Both the shoulder and the peak are annealed out with the same annealing rate suggesting that both are related to the same defect. It is clear from this figure that the absorption band is reduced drastically as the annealing temperature is reached 350 °C. The total integrated area of the absorption band is directly proportional to the concentration of the defect. The relative integrated area is thus equal to the relative concentration (N/N_o), where N is the concentration of the irradiation-induced defect at any giving annealing temperature and N_o is the concentration of the irradiation-induced

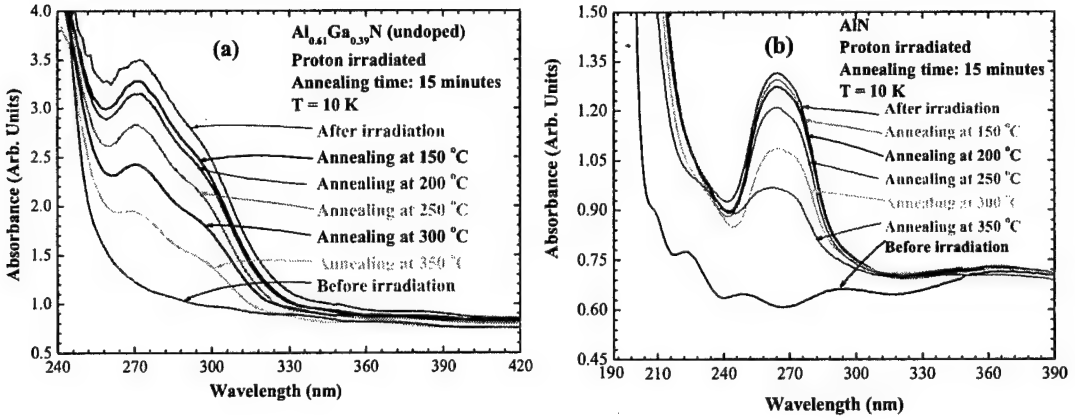

Fig. 20. Absorbance spectra of (a) $Al_{0.61}Ga_{0.39}N$ and (b) AlN thin films measured at 10K before and after proton irradiation. The rest of the spectra were recoded after the samples are irradiated and thermally annealed at various temperatures ranging between 150 and 350 °C. The samples were annealed for 15 min at each temperature.

defect before thermal annealing. The natural log of (N/N_o) is plotted in Fig. 21 as a function of annealing time for different annealing temperatures for both $Al_{0.61}Ga_{0.39}N$

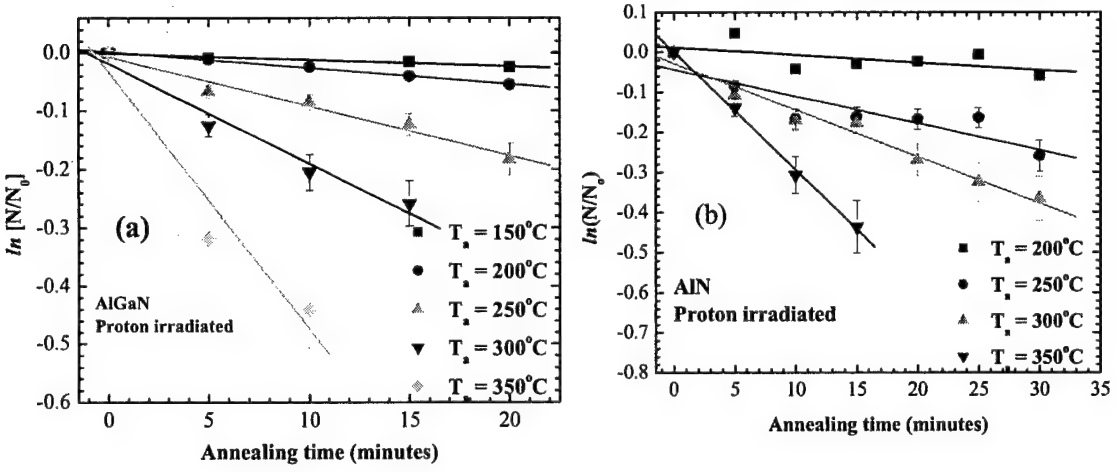

Fig. 21. The natural log of the relative defect concentration measured as a function of annealing time for (a) $Al_{0.61}Ga_{0.39}N$ and (b) AlN thin films at various temperatures. The solid lines in both figures represent the linear fits of the data. The slopes of the lines are the annealing rates [$\lambda(T)$] for various annealing temperature.

[Fig. 21 (a)] and AlN [Fig. 21 (b)] samples. The solid lines are due to the linear fits of the data. The variation of the defect concentration as a function of time at a constant temperature can be written as

$$\frac{dN}{dt} = -\lambda(T)N \ , \tag{4}$$

where $\lambda(T)$ is the annealing rate which takes the following form

$$\lambda(T) = \left(\frac{\nu_o}{N_j}\right)\exp\left(\frac{\Delta S}{k}\right)\exp\left(\frac{-\Delta H}{kT}\right). \tag{5}$$

Here T is the temperature, ν_o is the lattice frequency which is equivalent to Debye frequency, N_j is the average number of jumps before annealing, k is the Boltzmann constant, ΔS is the entropy and ΔH is the enthalpy associated with the migration process, i.e. the energy needed for the defect to overcome before annihilation. Thus, the slopes of the lines in Fig. 21 (a) and (b) represent $\lambda(T)$ at a given temperature. The natural log of $\lambda(T)$ is plotted as a function of (1/kT) in Fig. 22 for both $Al_{0.61}Ga_{0.39}N$ (solid squares) and AlN (solid diamonds) samples. ΔH is then obtained from the slopes of the linear fits of the data. The solid lines in Fig. 22 are the linear fits, which give $\Delta H = 0.410 \pm 0.023$ eV and $\Delta H = 0.445 \pm 0.037$eV for $Al_{0.61}Ga_{0.39}N$ and AlN, respectively. Since information on the values of ΔH for various native defects in III-nitride materials is scarce, the estimated values can be however compared to the vacancies in GaAs. The ΔH values obtained from Fig. 22 are in good agreement with the value of 0.4eV reported by Chiang and Pearson for V_{As} in GaAs. It is noted that these ΔH values are much smaller than those obtained for V_{Ga} (~2.0eV) in GaAs.

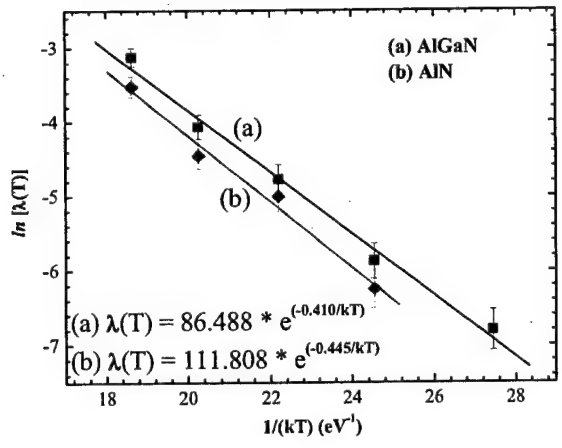

Fig. 22. The natural log of the annealing rate, $\lambda(T)$, measured as a function of 1/(kT) for both (a) $Al_{0.61}Ga_{0.39}N$ and (b) AlN thin films. The lines are the linear fits of the data and their slopes represent the enthalpy (ΔH) of the defect in both $Al_{0.61}Ga_{0.39}N$ and AlN.

Generally speaking, the presence of vacancies in semiconductors produces large distortions in the crystal. To verify this assertion, the FWHM of the presumably V_N absorption band in AlN [see Fig. 20 (b)] is measured as a function of temperature and the result is plotted in Fig. 23. The configuration coordinate approach is used to estimate the electron-phonon coupling that accompanied the transition responsible for the absorption

band in Fig. 20 (b). The solid line in Fig. 23 is the results of fitting the data with the expression

$$FWHM = \sqrt{8\ln(2)}\sqrt{S}\hbar\omega\sqrt{\coth(\hbar\omega/2kT)}\ , \qquad (6)$$

assuming the configuration coordinate curves for both the ground and excited sates of the localized center are identical parabolas with the same angular frequency. S in Eq. (6) is the Huang-Rhys factor, which is a measure of strong (S >> 1) or week (S << 1) electron-phonon coupling, ħω is the phonon energy, k is the Boltzmann constant, and T is the temperature. S and ħω were used as fitting parameters and the fitting procedure gives S = 23.9 and ħω = 47.8meV. The large value of S is an indication of a large electron-phonon coupling. The phonon energy of ħω = 47.8meV obtained here is in good agreement with the E_2 phonon mode energy of 52.8 meV measured for AlN material. Thus, Franck-Condon shift (d_{FC}) is estimated from S and ħω values to be $d_{FC} = S\hbar\omega = 1.142$ eV. This value is an indication of a large lattice relaxation associated with V_N vacancy in AlN. The small value of the enthalpy (~0.4eV), the large value of the Frank-Condon shift (~1.14 eV), and the annealing temperature range of 150 –350 °C are all in support of the identification of the absorption band observed below the conduction band (See Fig. 20) with the nitrogen vacancy in the proton irradiated AlGaN thin films.

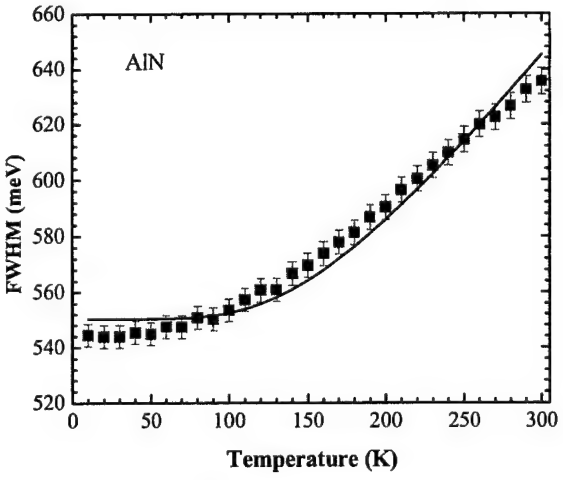

Fig. 23. The FWHM of the absorption band observed in AlN thin film [see Fig. 1(b)] as a function of temperature. The solid line is the result of fitting the data using Eq. (6).

In this section, we investigated the isothermal annealing effect on the absorption band, which attributed to the nitrogen vacancy, observed below the conduction band in proton irradiated $Al_{0.61}Ga_{0.39}N$ and AlN thin films. The Absorption band begins to anneal at temperatures as low as 150°C. The enthalpy associated with the migration process is estimated by studying the relative defect concentration as a function of time for different annealing temperatures and found to be ~0.4 eV. The electron-phonon coupling was also investigated by measuring the FWHM of the vacancy absorption band in AlN and it is estimated that the electronic transition is coupled to E_2 phone mode. Franck-Condon shift was estimated to be 1.42 eV, which indicates a large lattice distortion in the vicinity of the defect.

9. Local Vibrational Modes of Carbon-Hydrogen Complexes In Proton Irradiated AlGaN

In the fabrication of III-nitride based devices, ion bombardment is a very attractive tool for several technological steps, such as electrical and optical selective-area doping, dry etching, quantum well intermixing, etc. The performance of devices such as fast switches, and detector has been improved by subjecting them to well-controlled dose of particle irradiation. For example, proton bombardment induced defect with varying proton energy presents an opportunity for spatially varying carrier lifetime and free carrier densities in semiconductors, which has already successfully been implemented in Si device fabrication. Compare to the understanding of ion beam process in mature semiconductors (i.e. Si and GaAs), the understanding of the complex ion beam process in III-nitrides is still at its infancy. In order to avoid the deleterious effects of some of these particle-induced defects, and utilize the beneficial effects, depending on the application, much more work is essentially needed to understand the effect of irradiation on III-nitride material and device behaviors.

Local vibrational modes (LVMs) spectroscopy is a powerful tool in identifying impurities and dopant incorporation in semiconductors. Local vibrational modes are localized in both the real and frequency domains, giving rise to sharp peaks in infrared-absorption spectra. With this method, one can identify the lattice site of the impurity atoms due to the fact that LVMs of impurities are sensitively affected by the atomic structure surrounding the dopant or impurity atom. One typical example is that isotopic composition of the impurity and the surrounding atoms results in well-defined shifts in the vibrational frequencies.

This study is focused on investigating carbon-hydrogen complexes in proton irradiated AlGaN Local vibrational modes of C-H complexes in a series of undoped, Si-doped, and Mg-doped AlGaN samples grown on sapphire substrate by the metalorganic chemical vapor deposition technique (MOCVD) technique. The samples have been investigated by using 1MeV high-energy proton irradiation. LVMs spectra were recorded before and after proton-irradiating the samples. Thermal behavior of C-H complexes in AlGaN has been investigated by performing furnace thermal annealing. Furthermore, we report on the evolutions of C-H LVMs in proton irradiated sample as a function of irradiation dose and thermal annealed. The aging effect of the sample annealed at $T_a > 500^{\circ}C$ is also presented.

All the AlGaN samples, including unintentionally doped AlGaN, intentionally Si-doped and Mg-doped AlGaN used in this study were grown on sapphire substrate with AlN buffer layer using the MOCVD technique. The Al mole fraction ranges from 20% to 60%. The infrared-absorption measurements were performed with a BOMEM Fourier-transform spectrometer, which covers the spectral range of 450 - 4500 cm^{-1}, which is the range of interest to the present investigation. The temperature was controlled within $\pm 1.0K$ and the spectra were measured at both 300 K and 77 K.

The samples were irradiated with 1MeV protons and each sample received the following sequential doses $1.0x10^{16}$, $5.0x10^{16}$ and $10.0x10^{16}$ cm^{-2}. Infrared absorption measurements were performed before irradiation and after each of the above irradiation doses to investigate the evolution of C-H LVM spectra and their integrate areas. Furnace isochronal thermal annealing was performed on three samples to investigate the thermal annealing behavior of C-H complexes in as-grown and proton irradiated AlGaN thin films. The three samples used in this study are undoped $Al_{0.6}Ga_{0.4}N$ sample [denoted as

(A)], Si-doped $Al_{0.6}Ga_{0.4}N$ sample [denoted as (B)] and Mg-doped $Al_{0.4}Ga_{0.6}N$ sample [denoted as (C)]. All these samples were sandwiched between two boron nitride wafers to reduce the loss of nitride and ionization and heated in a continuous flow of N_2. For Mg-doped $Al_{0.4}Ga_{0.6}N$ sample, [sample (C)], it was heated at a sequence of temperatures from 100 to 900°C in steps of 50°C, and the annealing time was 2 minutes at $T_a \leq 700$°C and 15 minutes at $T_a \geq 750$°C. Infrared (IR) absorption measurements were made just after each annealing treatment on sample (C) as well as after waiting for periods of several days for each annealing treatment. This procedure allows us to observe the variation of the C-H LVM intensities and the aging effect. The aging effect is performed at each annealing temperature above 500 °C.

All the doped and undoped samples tested before and after proton irradiation in this study were found to contain five IR peaks in the spectral range of 2846 –2963cm^{-1}. Figure 24 shows the FTIR spectrum performed at 77K in the range of 2800 – 3050 cm^{-1} for the undoped $Al_{0.6}Ga_{0.4}N$ sample implanted with 1MeV proton and a dose of $1x10^{16}$cm^{-2}. This spectrum can be resolved into five peaks at 2849, 2870, 2902, 2918 and 2960 cm^{-1}. Based on a comparison between the LVM measurement in GaN and the calculated C-H frequencies in α-$Si_{1-x}C_x$: H, we ascribe these five peaks to symmetric and asymmetric stretching modes of CH_n (n=1,2,3) complexes in AlGaN. The absorption peak at 2848 cm^{-1} is attributed to a stretching mode of CH; the peaks at 2904 and 2916 cm^{-1} are attributed to a symmetric and an asymmetric stretching mode of CH_2, respectively; and the peaks at 2870 and 2960 cm^{-1} are attributed to symmetric and asymmetric stretching mode of CH_3. Table III summarize the LVMs of C-H complexes in AlGaN, GaN and α-$Si_{1-x}C_x$: H. From all the spectra of AlGaN samples that have been tested, we noted that the frequencies of these five peaks are sample dependent. It was found that the C-H stretching mode frequency could vary in different samples between 2846-2852 cm^{-1}, the CH_2 symmetric and asymmetric stretching modes vary between 2901-2906 and 2914-2922 cm^{-1} respectively, and the CH_3 symmetric and asymmetric stretching modes vary between 2869-2873 and 2957-2963 cm^{-1}, respectively.

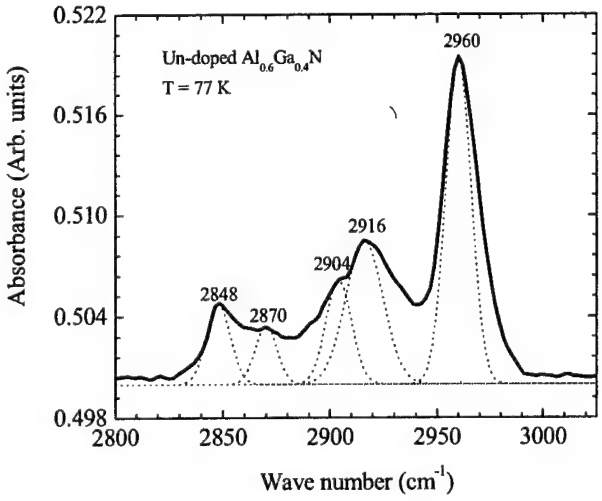

Fig. 24. Infrared absorption spectrum measured at 77K for a proton irradiated $Al_{0.6}Ga_{0.4}N$ sample. The IR absorption peaks are resolved into five peaks at 2848, 2870, 2904, 2916 and 2960 cm^{-1}. The solid line is the actual spectrum while the dotted lines are Guassians added to the spectrum for clarification.

Table III. Vibrational stretching mode frequencies of carbon-hydrogen complexes in AlGaN, Mg-doped GaN and α-$Si_{1-x}C_x$:H thin films measured at 77K. The AlGaN sample was irradiated with 1MeV proton and a dose of 1x10^{16} cm^{-2}. The unit of the frequencies is cm^{-1}.

	Stretching Mode	Measured frequencies in AlGaN	Measured frequencies in GaN	Measured frequencies in α-$Si_{1-x}C_x$: H	Calculated frequencies in α-$Si_{1-x}C_x$:H
CH		2848 ± 4	2853 ± 1	2860	2850
CH_2	Asymmetric	2916 ± 6	2923 ± 1	2890-2920	2949
CH_2	Symmetric	2904 ± 3	2900 ± 5	2870-2880	2902
CH_3	Asymmetric	2960 ± 3	2956 ± 2	2940-2960	2950
CH_3	Symmetric	2870 ± 3	2870 ± 5	2870-2880	2878

The LVMs spectra of Mg-doped $Al_{0.43}Ga_{0.57}N$ sample tested before and after proton irradiation were shown in Figure 25. Spectrum (1) in this figure was obtained from the as-grown sample. Spectrum (2) and (3) were obtained for this sample after irradiation with 1MeV protons and doses of 5x10^{16} and 1x10^{17} cm^{-2}, respectively. It is clear from this figure that the implantation of proton into AlGaN gives rise to a much more significant intensities variation of the CH_3 asymmetric stretching mode than that of other modes. All the other samples we tested in this study shows similar behavior.

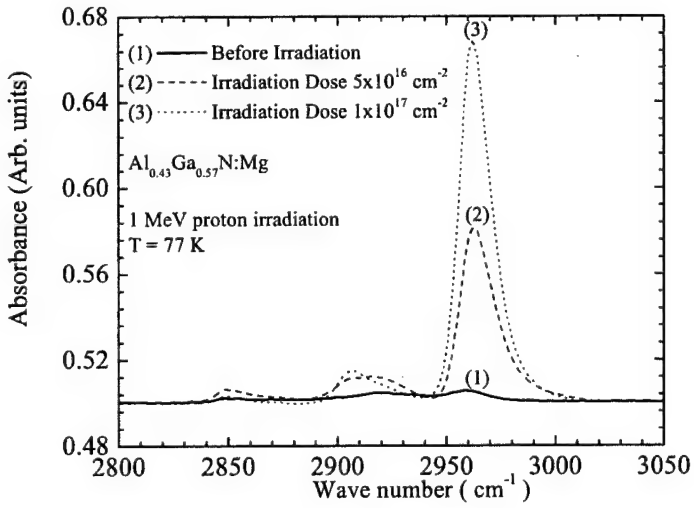

Fig. 25. Local vibrational mode spectra of C-H complexes measured at 77K for a Mg-doped AlGaN sample. Spectrum (1) was obtained for as-grown sample. Spectra (2), (3) were obtained for sample irradiated by 1MeV proton with doses of 5x10^{16} and 1x10^{17} cm^{-2}, respectively.

The evolution of the LVMs integrated areas of C-H complexes in undoped, Si-doped, and Mg-doped with different doses of proton is plotted in Fig. 26. Line (1) is obtained for undoped $Al_{0.6}Ga_{0.4}N$ sample, line (2) is for Mg-doped $Al_{0.43}Ga_{0.57}N$ sample, and line (3) is for Si-doped $Al_{0.56}Ga_{0.44}N$ sample. It is observed that the LVMs intensities of CH complexes are increased as the irradiation dose is increased in Mg and Si doped

AlGaN thin films in the entire irradiation range used in this study. In the doped materials, the hydrogen atoms seem to continue to form CH complexes without reaching the saturation stage. On the other hand, the intensities of the CH LVMs complexes in the undoped AlGaN sample were increased first and then start to decrease as the proton irradiation dose is increased above $5x10^{16}cm^{-2}$.

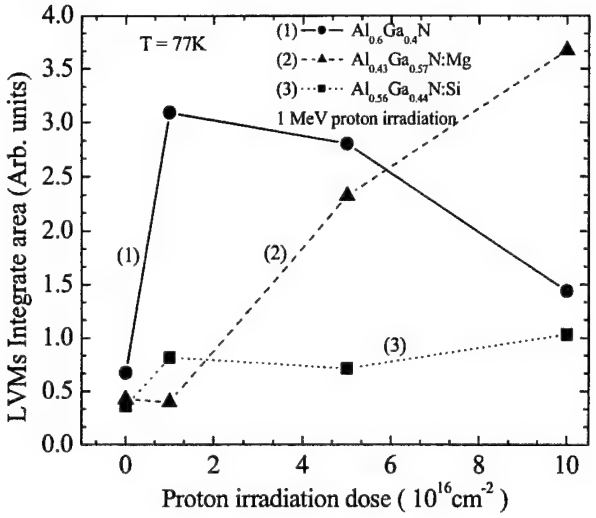

Fig. 26. The integrated areas of carbon-hydrogen LVMs in undoped, Si-doped, Mg-doped AlGaN samples plotted as a function of irradiation dose.

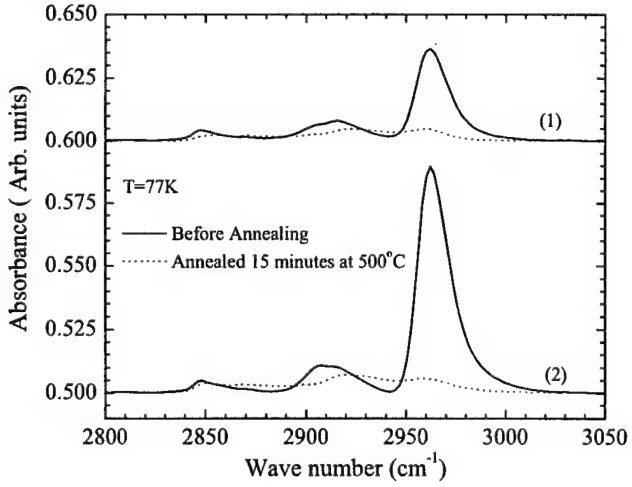

Fig. 27. Local Vibrational Modes spectra measured before annealing (solid line) and after 15 minutes annealing at 500°C (dot line) in sample (1), (2) are shown. Sample (1) is Si-doped as-grown $Al_{0.6}Ga_{0.4}N$. Sample (2) is un-doped $Al_{0.6}Ga_{0.4}N$ with 1MeV proton irradiation at the dose of $5x10^{16}cm^{-2}$. All the measurements were carried out at 77K.

Figure 27 shows infrared absorbance spectra of sample (A) (spectrum 1) and sample (B) (spectrum 2) measured before (solid line) and after 15 minutes thermal annealing at 500°C (dotted line). The thermal annealing behavior of LVMs spectra of C-H complexes in sample (C) is shown in Fig. 28(a) - (c). Figure 28(a) shows the LVMs

spectral behavior as the annealing temperature is changed. Figure 28(b) shows spectra for the same sample annealed at higher temperatures. These spectra were measured just after thermal annealing (dotted spectra) and several days after thermal annealing was performed (solid spectra). The data labeled (1) in Fig. 28(c) show the total integrated areas of CH LVMs in sample (C) tested just after each annealing treatment. While the data for the integrated areas labeled (2) in this figure were obtained after annealing the

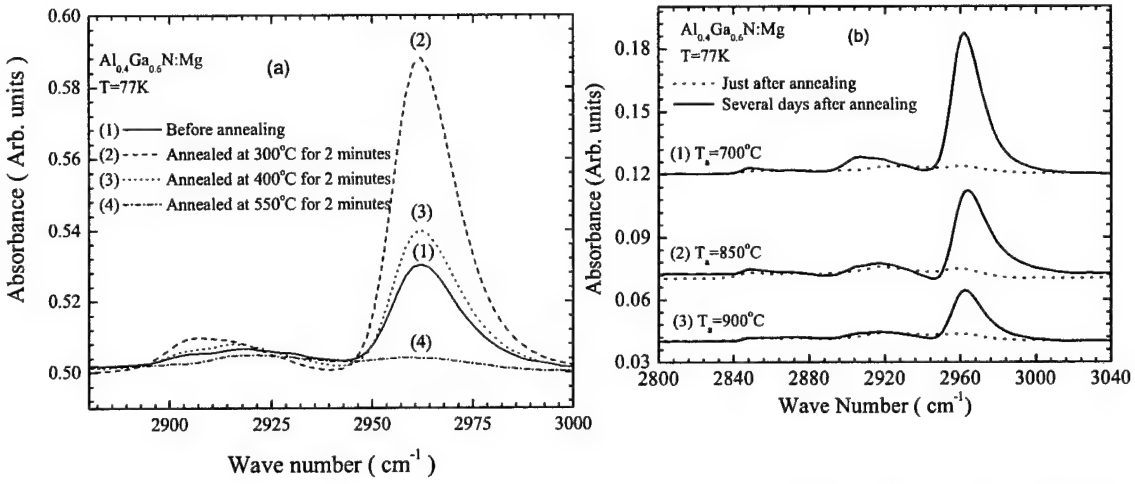

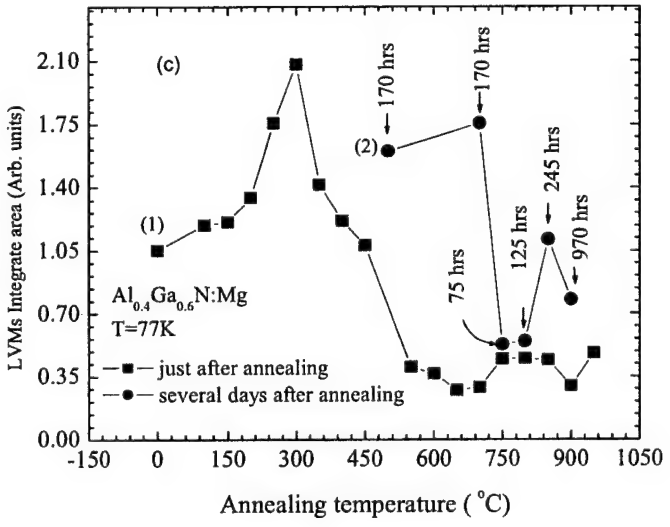

Fig. 28. (a) Local vibrational modes spectra of CH complexes measured at 77K in Mg-doped $Al_{0.4}Ga_{0.6}N$ sample measured after thermal annealing at T_a=300, 400, and 550 °C. (b) The same as (a) but T_a=700, 850, and 900 °C. The dotted lines represents the spectra measured just after thermal annealing while the solid lines represent the spectra measured several days after thermal annealing. (c) Total integrated areas of C-H LVMs measured for the Mg-doped $Al_{0.4}Ga_{0.6}N$ sample. Data labeled (1) were obtained after thermal annealing and data labeled (2) were obtained several days after thermal annealing. The number of hours in the graph represents the waiting periods used to measure the spectra after thermal annealing.

samples and waiting for periods of 170 hours or higher as indicated in the figure. The data labeled (1) in Fig. 28(c) clearly show an increase in the total integrated area as the annealing temperature is increased from 0 to 300 °C. As T_a is increased above 300 °C, the integrated area starts to decrease and essentially vanished at T_a above 600 °C. But then the CH LVMs seem to recover after waiting for a period of 170 hours or higher as indicated in the data labeled (2).The LVMs spectra of sample (C) in Fig. 28(b) were obtained just after each annealing (dotted spectra) and after waiting for a period of several days (solid spectra) at T_a = 700 (spectra 1), 800 (spectra 2) and 900 °C (spectra 3). It is obvious that a partial recovery of CH LVMs occurs when the samples were tested one week after thermal annealing. It is also noted that the general trend is that the total integrated areas of the C-H LVMs is decrease as the annealing temperature is increased above 300 °C for both before and after the aging [see Fig. 28(c)].

It is known that atomic hydrogen is a fast diffuser and can effectively interact with defects in the host crystals. Theoretical studies based on the density functional approach within the local density approximation for wurtzite and zinc-blende lattices have indicated that the dominant charge state of atomic hydrogen in interstitial solution in GaN is H^+ or H^- depending upon the positions of the Fermi level, with H^0 always being less stable.[35-38] H^+ is the lowest energy state in p-type GaN and H^- is the lowest state in n-type GaN. H^+ and H^0, on the other hand, are found to be much more mobile than H^-. These studies also indicate that H can form complex structures by binding with neutral dopants such Mg acceptor or Si donor on the Ga sublattice as well as with residual impurities such as C. Hydrogen can also be in the form of multi-atomic hydrogen related centers (H_2, C-H_n, n=1,2,3 etc.). Neutral interstitial molecular H_2 has a lower formation energy than all three atomic states and was predicted to be energetically preferred for a limited range of Fermi energies near the middle of the band gap. Calculation also indicates that clustering of hydrogen atoms might occur in p-type GaN. Energetic ion bombardment can produce gallium (V_{Ga}) and nitrogen (V_N) vacancies and interstitial by atomic collisions. The energetic H will initially come to rest at sites with local energy minima. Depending on its mobility, H will either remain at metastable sites or move to lower energy sites at lattice defects or dopants. In the parallel system of AlGaN, we assume that hydrogen states have the same behaviors.

In GaN, carbon most likely occupies the nitrogen site. The C-H defect complexes formed when hydrogen passivates substitutional C_N in GaN. Hydrogen has been found to be located at a bond-center site between the C and the neighboring Ga atoms as is the case for GaAs and InAs. The experimental results shows that the CH_n LVM frequencies in AlGaN are similar to that in GaN thin film. This proves that C-H complexes in AlGaN have the same atomic configuration similar to that in GaN. The present experimental result show a slight difference in the LVM frequencies of the C-H complexes in AlGaN as compared to those in GaN. This difference is expected since Al atoms were added to the crystal, and consequently the atomic structure around C-H complexes in AlGaN is different from that of GaN due to the fact that LVMs are highly sensitively to the surrounding atomic structures. Additionally, we observed that LVMs frequencies in AlGaN are sample dependent. This sample dependency could be explained in terms of

the presence of dislocations. The strains associated with dislocation are usually sample dependent and can affect the LVMs in a way that their frequencies are sample dependent.

In the formation of $C\text{-}H_n$ (n=1,2,3), n bonds of C-Ga need to be broken for the hydrogen to be incorporated. It is obviously that more energy is needed if more C-Ga bonds are broken. Therefore, after the implantation of proton, the possibility to form C-H complexes is much larger than that of forming $C\text{-}H_2$ and $C\text{-}H_3$, however we observed in all the samples tested in this proton irradiation study that the concentration of $C\text{-}H_3$ is much higher than the concentration of $C\text{-}H_2$ and C-H. This leads to the assertion that hydrogen prefers to form $C\text{-}H_3$ in proton irradiated AlGaN. A possible explanation for this behavior is that there is a substantial number of V_{Ga} in the vicinity of C_N. This is quite possible since the energetic proton bombardment can produce V_{Ga} by atomic collisions, which is a good background to form $C\text{-}H_n$ for $n > 1$ before V_{Ga} is annihilated.

In Fig. 26, we have shown the total integrated areas of CH LVMs as a function of irradiation dose for the three different samples (undoped, Mg-doped and Si-doped). The LVM results qualitatively provide useful information on the concentration of carbon impurity and the C-H complexes formation rate with proton irradiation dose. For different samples, it is obviously that they have different concentration of carbon impurity. For example, if a samples contains a large concentration of C and by adding H^+ though irradiation, one would expect to observe an increase in the concentration of the C-H complex defect. This is demonstrated in Fig. 6. In particular, the data labeled (2) indicate that this sample contains a larger carbon concentration as compared to the other two samples. For samples such as the undoped and Si-doped samples, the carbon concentration seems to be much lower as judged by the formation of the C-H complex defects. The reduction of the total integrated areas in the latter two samples [data labeled (1) and (3)] might be due to the decomposition of the C-H complexes by proton irradiation. This process is quite feasible in samples where the carbon atoms are completely compensated. Hence, excess proton irradiation will cause partial dissociation of C-H complexes. For the Mg-doped AlGaN samples, the dominant charge state of H is H^+ which is a faster diffuser, therefore, part of the H^+ will form neutral complex with Mg acceptor and part of H^+ will be attracted by the C_N which is also an acceptor. If a V_{Ga}, which is an acceptor with negative charge state, is near C_N, it may enhances the chances of forming C-H complexes since H^+ prefer to attach itself to dangling bonds available at the vacancy site. For Si-doped samples, the dominant charge state of H is H^- which is less mobile compare to its other two atomic states. The formation of the $C\text{-}H_n$ (n=1,2,3) complexes by the diffusion of H^- towards substitutional carbon is unlikely in n-type AlGaN since both are ionized acceptors whose negative charges repel one another. The V_{Ga} near C_N will also repel H^-. For the undoped samples, major part of the energetically H atoms diffuse and combine with carbon to form C-H complexes. From this discussion, it is clear that C-H complexes as judged from the intensity of their LVMs are formed with higher rates in the proton irradiated undoped as compared the Mg and Si-doped samples. Figure 26 clearly show that formation rate of C-H complexes in the Si-doped sample is much lower than that in updoped and Mg-doped samples.

Figure 28 (a) and (b) show the thermal annealing effect on C-H LVMs. The asymmetrical stretching mode of CH_3 is affected dramatically by thermal annealing as compared to other stretching modes of CH2 and CH. This means that CH_3 is thermally unstable. It is observed from Fig. 28(c) that the LVMs integrated area of C-H complexes

in Mg-doped sample is increased with increasing annealing temperature and it reaches a maximum value after annealing the sample at 300 °C. This proves that C-H complexes in AlGaN are stable below 300 °C. Thermal annealing at T_a < 300 °C seems to help the formation of C-H. The C-H LVM intensities decrease after thermal annealing treatment at T_a > 300°C due to the dissociation of C-H complexes. After the thermal dissociation of C-H complexes, H either lose an electron and becomes H^+, which could have a higher probability of recombining with C^- and reforming the passivated complexes, or it captures a second electron to form H^-. This of course will not recombine with C^-, and it is likely to migrate further away due to Coulomb repulsion and could eventually form either a molecule by combining with an H^+ or a larger H cluster or aggregate. C-H complexes seem to be completely depleted at T_a > 600°C.

To illustrate that the observed LVMs are due to C-H complexes, we cut two pieces from an $Al_{0.2}Ga_{0.8}N$ wafer and one piece was irradiated with 1 MeV protons and the other was irradiated with 1MeV electrons (dose = $1x10^{17}cm^{-2}$). The results are shown in Fig. 29. The solid line is the spectrum obtained from the samples before irradiation, the dashed line is the spectrum obtained for the proton irradiated sample, and the dotted line is the spectrum obtained from the electron irradiated sample. It is clear that proton irradiation increases the formation of C-H complexes as judged by the large increase in the stretching mode frequency of the CH_3 complex. An increase of the stretching mode frequencies for CH_2 and CH is also observed. However, the electron irradiated sample shows a noticeable decrease in the CH_3 stretching mode. This clearly demonstrates that electron irradiation break up the CH_3 complex in good agreement with others. There is an increase of the CH_2 and CH concentrations in the electron irradiated sample as seen from the increase in the area under the LVMs stretching modes. This is most likely due to the fact that CH_3 is decomposed into C, H, CH, and CH_2. This behavior is observed in several samples. Additionally, Hall effect measurements show a slight increase in the carrier concentration in the electron irradiation samples. This does not seems to be universal since a few samples show a slight decrease in the carrier concentration after electron irradiation.

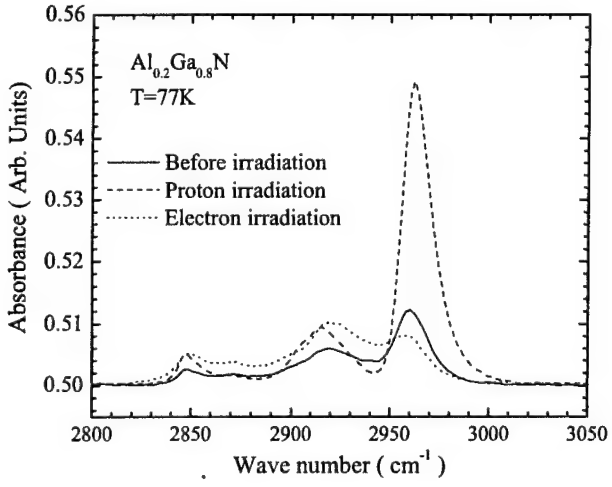

Fig. 29. Local vibrational modes spectra measured for two samples cut from the same $Al_{0.2}Ga_{0.8}N$ wafer. The solid line is the spectrum obtained for both samples before irradiation, the dashed line represents the spectrum obtained for the proton irradiated sample (dose=$6x10^{16}cm^{-2}$), and the dotted line represent the spectrum obtained for the electron irradiated (dose=$1x10^{17}cm^{-2}$) sample.

In this section we presented the local vibrational modes spectra of C-H complexes in proton implanted AlGaN grown by MOCVD technique. Five distinctive C-H LVM frequencies were observed around 2848, 2870, 2904, 2916 and 2960 cm^{-1}, which are slightly different from those observed in GaN, are related to stretching symmetrical and asymmetrical vibrational modes of CH_n (n=1,2,3). The evolution of the integrated areas of CH LVMs in proton irradiated samples is presented as function of irradiation dose. In the Mg-doped AlGaN sample, hydrogen atoms (proton) seem to continue to form C-H complexes without reaching the saturation stage in the whole irradiation dose used in this study. This may be due to the fact that carbon is present with a high concentration. Si-doped samples on the other hand show a slight increase in the CH LVM intensities as the dose is increased. Thermal annealing at temperature around 500°C is sufficient enough to dissociate most of the C-H complexes in AlGaN thin film. However, a partial recovery of the CH LVMs is observed in thermally annealed samples at $T_a > 500$ °C. This intriguing behavior is explained in terms of C-H recombination, which strongly suggests that H atoms remain trapped in the sample even after C-H decomposition. However, the integrated areas of the C-H LVMs are decreased after thermal annealing and aging as the annealing temperature is increased. While proton irradiation cause a drastic increase in the CH3 LVM, electron irradiation cause the opposite effect suggesting strongly that the observed LVMs are truly due to CH complexes.

10. List of publications, professional activities and students:

A. Papers in technical journals and symposia:

1. *"Response to 'Comment on "Thermal Annealing Efect on the Intersublevel Transitions in InAs Quantum Dots [Appl. Phys. Lett. 78, 2196 (2001)]"'"* Y. Berhane, M. O. Manasreh, H. Yang, and G. J. Salamo, Appl. Phys. Lett. **80**, 4869-4870 (2002).
2. "*Intersubband Transitions in InGaAs/InAlAs Multiple Quantum Wells Grown on InP Substrate.*" Qiaoying Zhou, M. O. Mansreh, B. D. Weaver, and M. Missous, Materials Research Socity, vol. **692**, 253-258 (2002).
3. "*Local Vibrational Modes of Carbon-Hydrogen Complexes in Proton Irradiated AlGaN thin films."* M. O. Manasreh and B. D. Weaver, Materials Research Socity, vol. **692**, 403-409 (2002).
4. "*Thermal Annealing Effect on Carbon-Hydrogen complexes in AlGaN thin films.*" M. O. Manasreh and D. W. Weaver, Materials Research Socity, vol. **692**, 581-586 (2002).
5. "*Optical Absorption of Deep Defects in Proton Irradiated AlGaN thin films.*" Q. Zhou, J. Chen, M. Pophristic, I. Ferguson, S. Kucheyev, C. Jagadish, and B. D. Weaver, Materials Research Socity 2001 Fall Meeting, Symposium "H" (accepted).
6. "*Thermal Annealing Effect on Nitrogen Vacancy in Proton Irradiated AlGaN.*" Qiaoying Zhou and M. O. Manasreh, Appl. Phys. Lett. **80**, 2072-2074 (2002).

7. *"Structural Disorder in Ion-Implanted AlGaN."* S. O. Keucheyev, S. J. Williams, J. Zou, G. Li, C. Jagadish, M. O. Manasreh, P. Pophristic, S. Guo, and I. T. Ferguson. Appl. Phys. Lett. **80**, 787-789 (2002).

8. *"Observation of Nitrogen Vacancy in $Al_xGa_{1-x}N$ thin films."* Q. Zhou, M. O. Manasreh, M. Pophristic, and I. Ferguson, Appl. Phys. Lett. **79**, 2901-2903 (2001).

9. *"Thermal Annealing Effect on Intersublevel Transitions in InAs Quantum dots."* Y. Berhane, M. O. Manasreh, H. Yang, and G. J. Salamo, Appl. Phys. Lett. **78**, 2196-2198 (2001).

10. *"Proton and He^+-ion Radiation Effect on Intersubband transitions in GaAs/AlGaAs Multiple Quantum Wells."* Y. Berhane, M. O. Manasreh, B. D. Weaver, H. H. Tran, and C. Jagadish, SPIE Proceedings, Vol **4454**, p.85-93 (2001) **(Invited)**.

11. *"He^+-Ion Irradiation Effect on Intersubband Transitions in GaAs/AlGaAs Multiple Quantum Wells."* Y. Berhane, M. O. Manasreh, and B. D. Weaver, J. Appl. Phys. **89**, 3517-3519 (2001), **Rapid Communication**.

12. *"Disorder-Effects in Reduced Dimensional and Quanantum Electronics."* B. D. Weaver, R. Magno, E. M. Jackson, R. Wilkins, S. Shojah-Ardalan, A. C. Seabaugh, B. Brar, M. O. Manasreh, and Y. Berhane, AIP Conference Proceedings Vol. **552**, 1210-1216 (2001) **(Invited)**.

13. *"Optical Absorption Properties of Bulk **SiC**."* K. Miller, Hong-Xia Zhang, M. O. Manasreh, Z. C. Feng, and I. Ferguson, Materials Research Society, Vol. **640**, page H5.23 (2001).

14. *"Carbon-Hydrogen Complexes in Metalorganic Chemical Vapor Deposition Grown **GaN**."* M. O. Manasreh, C. A. Tran, and I. Ferguson, Materials Research Society, Vol. **639** (2001)

15. *"Thermal Annealing Recovery of Intersubband Transitions in Proton Irradiated **GaAs/AlGaAs** Multiple Quantum Wells."* F. Hegeler, M. O. Manasreh, C. Morath, P. Ballet, H. Tang, G. J. Salamo, H. H. Tan, and C. Jagadish, Appl. Phys. Lett. **77**, 2867-2869 (October 2000).

16. *"Introduction to Defects and Structural Properties of III-Nitride Semiconductors."* M. O. Manasreh in "III-Nitride Semiconductors: Defects and Structural Properties" (Elsevier, Amsterdam, The Netherlands, 2000), chapter 1, pp 1- 23.

17. *"Introduction to **InP** and related Compounds."* M. O. Manasreh, in "Optoelectronic Properties of Semiconductors and Superlattices", (Gordon & Breach, Newark, NJ, 2000), Vol. **9**, chapter one, pp.1-7.

18. *"Fast Neutron Irradiation Effects on the Interband Transitions in **InGaAs/AlGaAs** Multiple Quantum Wells."* M. O. Manasreh and S. Subramanian, Materials Research Society, Vol. **607**, 525 - 528 (2000).

19. "*Degradation of Intersubband Transitions in Electron Irradiated **GaAs/AlGaAs** Multiple Quantum Wells with Superlattice Barriers.*" C. Morath, M. O. Manasreh, H. S. Gingrich, H. J von Bardeleben, P. Ballet, J. B. Smathers, and G. J. Salamo, Materials Research Society, Vol. **607**, 503 - 508 (2000).

20. "*Thermal Annealing Recovery of Intersubband Transitions in Proton Irradiated **GaAs/$Al_{0.3}Ga_{0.7}As$** Multiple Quantum Wells.*" H. S. Gingrich, C. Morath, M. O. Manasreh, P. Ballet, J. B. Smathers, G. J. Salamo, and C. Jagadish, Materials Research Society, Vol. **607**, 217-222 (2000).

21. "*Intersubband Transitions in **InGaAs/AlGaAs** Multiple Quantum Wells and Their Behavior Under Proton and Electron Irradiation.*" M. O. Manasreh, P. Ballet, J. B. Smathers, G. J. Salamo, C. Jagadish, and H. J. von bardeleben, Submitted for presentation and publication in the 5th International Conference on Intersubband Transitions in Quantum Wells, Bad Ischl, Austria, September 7-11 (1999).

22. "*Localized Vibrational Modes of Carbon-Hydrogen Complexes in **GaN**.*" M. O. Manasreh, J. M. Baranowski, K. Pakula, H. X. Jiang and Jingyu Lin, Appl. Phys. Lett. **75**, 659-661 (1999).

23. "*Proton Irradiation Effects on the Intersubband Transition in **GaAs/AlGaAs** Multiple Quantum Wells with Bulk or Superlattice barriers.*" M. O. Manasreh, P. Ballet, J. B. Smathers, G. J. Salamo, and C. Jagadish, Appl. Phys. Lett. **75**, 525-527 (1999).

24. "*Electron Irradiation Effects on the Intersubband Transitions in **InGaAs/AlGaAs** Multiple Quantum Wells.*" M. O. Manasreh, H. J. von Bardeleben, A. M. Mousalitin, and D. R. Khokhlov, J. Appl. Phys. **85**, 630-632 (1999). **Rapid Communication.**

B. Books and Symposia:

1. **"Optoelectronic Properties of Semiconductors and Superlattices."** A book series edited by M. O. Manasreh (Taylor and Francis, transferred from Gordon and Breach).
   - **Volume 9:** *"InP and Related Compounds: Materials, Applications and Devices."* Volume Editor: M. O. Manasreh, (May 2000).
   - **Volume 10:** "*Vertical Cavity Surface Emitting Lasers and Their Applications.*" Volume editors: J. Cheng and N. K. Dutta, (May 2000).
   - **Volume 11:** **"***Defects in Optoelectronic Materials.***"** Volume Editor: K. Wada, (Dec 2001).
   - **Volume 12:** **"***II-VI Semiconductor Materials and Their Applications."* Volume Editor: Maria Tamargo, (April 2002).
   - **Volume 13:** *"III-V Nitride Semiconductors: Optical Properties I."* Volume Editors: H. X. Jiang and M. Omar Manasreh, (Nov 2002).
   - **Volume 14:** *"III-V Nitride Semiconductors: Optical Properties II."* Volume Editors: H. X. Jiang and M. Omar Manasreh, (Nov 2002).

Volume 15: *"Properties and Applications of Silicon Germanium Carbide Alloys: Recent Developments."* Volume editors: Sokrates Pantelides and Stefan Zollner, (Nov 2002)

Volume 16: *"III-V Nitride Semiconductors: Applications and Devices."* Volume Editors: E. T. Yu and M. Omar Manasreh, (Nov 2002).

Volume 17: **"***Lead Chalcogenides: Physics and Applications***."** Volume Editor: D. Khokhlov, (Nov 2002).

Volume 18: **"***Microprobe Characterization of Optoelectronic Materials***."** Volume Editor: J. Jimenez, (Nov 2002).

Volume 19: **"***III-V Nitride Semiconductors: Growth and Substrate Issues."* Volume Editors: M. Omar Manasreh and Ian Ferguson, (Nov 2002).

2. **"III-V Nitride Semiconductors: Electrical, Structural and Defects Properties."** Edited by M. Omar Manasreh, (Elsevier, Amsterdam, December 2000).

3. **"Progress in Semiconductor Materials II: Electronic & Optoelectronic Applications."** A symposium is organized by B. D. Weaver, M. O. Manasreh, S. Zollner, and C. Jagadis for the Materials Research Society (Fall 2002).

4. **"Progress in Semiconductor Materials for Optoelectronic Applications."** A symposium organized by M. O. Manasreh, E. D. Jones, K. D. Choquette, and D. Friedman for the Materials Research Society (Fall 2001). Volume **692.**

5. **"Infrared Applications of Semiconductors III."** Edited by M. O. Manasreh, B. Standler, I. Ferguson, and Y. Zhang. (Materials Research Society, Pittsburgh, 2000), Volume **607.**

C. Professional Papers at Regional, National, and International Meetings:

1 "Optical Absorption Properties of Doped and Undoped Bulk SiC." K. Miller, Q. Zhou, and M. O. Manasreh. Third annual NASA-PURSUE Conference, Albuquerque, NM, 21-22 April 2001.

2 "α-Particel Irradiation Effect on Intersubband Transitions in GaAs/AlGaAs Multiple Quantum Wells." M. Martinez, Y. Berhane, and M. O. Manasreh. Third annual NASA-PURSUE Conference, Albuquerque, NM, 21-22 April 2001.

3 "Irradiation Effects on Intersubband Transitions in **InGaAs/AlGaAs** Multiple Quantum Wells." M.O. Manasreh, H. J. von Bardeleben, A. M. Mousalitin, D. R. Khokhlov , and Chennupati Jagadish, Bull. Am. Phys. Soc. **44**,220 (1999).

4 "Localized Vibrational Mode Spectroscopy of Impurities and Dopants in III-V Semiconductors." M. O. Manasreh, Bull. Am. Phys. Soc. **44**,1338 (1999).

D. Invited Talks and Presentations:

1. "Infrared Appliations of III-V semiconductor Superlattices and Nanostructures." Presented to the Department of Electrical Engineering, University of California-Riverside, 5 April 2002.

2. "Radiation Effect on III-V Optoelectronic Materials and Device." Presented to
   a) ARO, Durham, NC, 9 October 2001.
   b) Department of Physics, University of Puerto Rico, Rio Piedras, PR, 5 Feb 2002.
3. "Optical Properties of Dopants and impurities in III-Nitride Materials." Presented to DARPA workshop on "III-Nitride UV Emitters." Arlington, VA, 9-10 April 2001.
4. "Radiation Effect on Intersubband Transitions In GaAs/AlGaAs Multiple Quantum Wells." A seminar presented to the department of Electrical and Computer Engineering, University of New Mexico, Albuquerque, NM, 9 February 2001.
5. The following lectures were presented to the Petra School of Physics, University of Jordan, Amman, Jordan during the period of 16 – 22 September 2000:
   a) "Intersubband Transitions in III-V Semiconductor Quantum Wells and Their Applications to Long Wavelength Infrared Detectors."
   b) "Radiation Effects on Intersubband transitions in Quantum Wells."
   c) "Optical Properties of III-Nitride Semiconductors."
6. "Space-Based Optoelectronic Materials and Device." A seminar presented to the Department of Electrical and Computer Engineering, University of New Mexico, 10 March 2000.

E. Students supported by the grant:

1. Yosief Berhane (M.S. Student)
2. Jing Chen (Ph. D. student)
3. Qiaoying Zhou (Ph. D. Student)
4. Kristina Miller (undergraduate student)
5. Mario Martinez (undergraduate student)
6. Tony Peredo (undergraduate student).
7. Robert Barbera Jr. (undergraduate student)